

**DISENTANGLING MODES WITH CROSSOVER
INSTANTANEOUS FREQUENCIES BY SYNCHROSQUEEZED
CHIRPLET TRANSFORMS, FROM THEORY TO APPLICATION**

ZIYU CHEN AND HAU-TIENG WU

ABSTRACT. Analysis of signals with oscillatory modes with crossover instantaneous frequencies is a challenging problem in time series analysis. One way to handle this problem is lifting the 2-dimensional time-frequency representation to a 3-dimensional representation, called time-frequency-chirp rate (TFC) representation, by adding one extra chirp rate parameter so that crossover frequencies are disentangled in higher dimension. The chirplet transform is an algorithm for this lifting idea. However, in practice we found that it has a stronger “blurring” effect in the chirp rate axis, which limits its application in real world data. Moreover, to our knowledge, we have limited mathematical understanding of the chirplet transform in the literature. Motivated by real world data challenges, in this paper, we propose the synchrosqueezed chirplet transform (SCT) that gives a concentrated TFC representation that the contrast is enhanced so that one can distinguish different modes even with crossover instantaneous frequencies. We also analyze chirplet transform and provide theoretical guarantee of SCT.

1. INTRODUCTION

Time series (or signals) are ubiquitous in almost all scientific fields. Often, the observed/recorded signal is composed of multiple components. Due to the nonstationary dynamics of our natural system, if the component is oscillatory, it usually oscillates with time-varying amplitudes, frequencies and even the oscillatory patterns. On the other hand, if the component is stochastic, it could be a nonstationary random process with time-varying statistical properties. These time-varying quantities encode rich information about the dynamics of the underlying system of interest. By properly extracting and parsing these time-varying quantities, we could peek into nature and decode the underlying dynamics. In this paper, we focus on analyzing signals with oscillatory components and extracting the dynamics.

To properly extract and parse the time-varying quantities of each oscillatory component from the input signal is however not easy. For example, due to the nonstationarity, the traditional Fourier transform cannot properly capture such information, since the Fourier transform is a global operator. An intuitive and successful solution to handle the nonstationarity is “divide-and-conquer”. By dividing the signal into pieces, and assuming that each piece is stationary, we could apply Fourier transform over each piece to capture the nonstationarity. This intuitive idea has led to a rich field called time-frequency (TF) analysis, where the “spectrum” at each moment is evaluated so that the time-varying frequency and amplitude could be evaluated. It includes various algorithms, ranging from linear-type, polynomial-type to nonlinear-type algorithms. For example, the short-time

Fourier transform (STFT), the continuous wavelet transform (CWT) and the S transform are linear-type algorithms. The Wigner-Ville, Cohen's class and affine class are bilinear-type algorithms [17]. The polynomial Wigner-Ville distributions are polynomial-type algorithms [4, 5, 2]. The reassignment method (RM) [1], the synchrosqueezing transform (SST) [12] and its generalizations [28], the Blaschke decomposition [27], and the empirical mode decomposition (EMD) [20] and its variations are nonlinear-type algorithms. We refer readers with interest to a recent review of the topic [39]. In short, these algorithms convert an input signal into a TF representation and/or oscillatory components. From the output, we could more efficiently visualize or extract different time-varying properties of the input signal. While the linear-type algorithms have been widely applied, one well-known property shared by these algorithms is the uncertainty principle. This uncertainty principle leads to a blurred TF representation so that the information of interest, like the ridges [9], is of low contrast. This may cause troubles in some applications. This problem can be handled by nonlinear-type approaches; for example, RM [1] and SST [12] were invented for the sake of sharpening the TF representation so that its contrast is enhanced. Even more, signals with chirp components can be further enhanced by higher order SST [29].

While we have advanced the analysis tools from various fronts in the past 20 years, there are still several challenges. In this paper, we focus on the specific crossover frequency challenge. Recall that most of the above algorithms are based on the assumption that different oscillatory components have "well-separated" time-varying frequencies in the TF plane. Mathematically, this well-separation condition is defined in the following way. Suppose a signal is a superposition of multiple *intrinsic-mode-type* (IMT) functions [12]:

$$f(t) = \sum_{k=1}^K f_k(t) = \sum_{k=1}^K A_k(t) e^{2\pi i \phi_k(t)},$$

where $A_k(t) > 0$ and $\phi'_k(t) > 0$ models the time-varying amplitude (or called amplitude modulation (AM)) and time-varying frequency (or called instantaneous frequency (IF)) of the k -th IMT component $f_k(t)$, with some regularity assumptions. Suppose for any $k \neq j$, we have $|\phi'_k(t) - \phi'_j(t)| \geq \Delta$ for some constant $\Delta > 0$ for all t , the signal f satisfies the well-separation condition. This is the minimal assumption we need for most TF analysis tools mentioned above. When this well-separation condition is broken, for example, when the time-varying frequencies of two oscillatory components are too close, or even crossover, the algorithm fails. Mathematically, when $\phi'_k(t) = \phi'_l(t)$ for some t , we say that the k -th and l -th components have *crossover IFs*.

See Figure 1 for a synthetic signal as an example, where $f(x) = f_1(x) + f_2(x)$, where $f_1(x) = e^{2\pi i \cdot 4x^2}$, and $f_2(x) = e^{2\pi i[-\pi x^2 + (24+6\pi)x]}$, $x \in [1, 5]$, with such a crossover frequency phenomenon. The signal is sampled at 100Hz. Note that in this simple case, the chirp rates are not time-varying, and their IFs have a crossing point at $t_0 = 3$ and $\xi_0 = 24$. Figure 1 gives the time-frequency representations determined by STFT, RM, SST, and 2nd-order SST with the window $g_0(x) = e^{-\pi x^2}$. Clearly, the spectrogram (the magnitude of the STFT of the signal) and the TF representation determined by SST are blurred as expected, and the TF representation is sharpened after applying RM and the 2nd-order SST. However,

during the period that two IFs crossover, all approaches encounter troubles, and we need a new approach to handle it.

Recently, some methods have been proposed to handle signals with crossover frequencies. In [22], an IF estimator based on the linear least square fitting and the Viterbi algorithm was introduced. A quasi maximum likelihood - random samples consensus algorithm was proposed for the IF estimation of overlapping signals in the TF plane [15]. The chirplet transform (CT) was introduced in [24, 25, 26], which gives rise to a three dimensional parameter space, i.e., time, frequency (scale) and chirp rate that includes the TF plane (of the STFT) or the time-scale plane (of the CWT) as a subspace. Its discretization was later studied in [40] with several generalizations [6, 35] and applications [37, 11, 16, 19, 18], which is a non-exhaustive list. Besides its common application to estimate chirp rates, with the extra chirp rate dimension, it is possible to apply it to “see through” the crossover IFs. Such potential was confirmed in two recent papers. In [41], CT was employed to estimate IFs and chirp rates of a signal that can separate crossing IFs in the time-frequency-chirp rate (TFC) space. The CT was also employed to retrieve modes with crossover IFs from a signal with mathematical theorems in [21]. We shall mention two relevant papers that also depend on chirplet. In [8], the authors propose a multiscale chirplet method to “detect waves”, where the chirplet refers to atoms that oscillate with linearly varying frequency (fixed chirp rate) and exist in short (dyadic) time intervals. In [7], the authors propose a tight frame of “chirplet” as in [8] for the reconstruction of chirps; however, they do not deal with the problem of decomposing a multi-component signal or of estimating the instantaneous frequency and chirp rate.

While CT has been proposed to analyze signals with crossover IFs, there are several interesting open problems. First, the TFC representation determined by CT with the window g_0 is also impacted by the uncertainty principle; that is, the TFC representation is blurred. See the synthetic example in Figure 1. It seems that the “blurring” of the TFC representation is not improved compared with the spectrogram, particularly after projecting it onto the TF domain. Particularly, while at time $t_0 = 3$ and frequency $\xi_0 = 24$, the TFC representation on the chirp rate axis gives a separation of two components. However, the magnitude at the chirp rate 0 is nontrivial, which blurs the available information. It is thus beneficial if we could enhance the TFC representation for some specific applications. This blurring effect also raised our curiosity about the theoretical properties of CT. For example, if the input signal is L^1 , is the TFC representation in the chirp rate axis continuous and decays to 0, and what is the decay rate? If it decays fast, does CT map a L^2 function to a L^2 function? However, to our knowledge, the theoretical property of CT is less studied in the literature. In this paper, we seek to answer these questions, at least partially, and provide a practical algorithm to separate components with crossover IFs from a multicomponent signal. We propose to combine the “squeezing” idea with CT, and synchrosqueezed chirplet transform (SCT) that gives a sharper TFC representation of a signal, even if the signal has crossover IFs, from which one can separate different components. In addition to providing several theoretical properties of CT and a theoretical guarantee of SCT, we provide a series of numerical experiments with real data illustration. We shall mention that a seemingly similar squeezing idea has been shown in [42]. However, despite the nomination “squeeze”, the squeezing part was only applied to the frequency axis

that is based on the chirp rate information and only the TF representation was considered, and only limited theoretical analysis of the squeezing step is provided. Last but not the least, the Matlab code used in this paper is made public for the reproducibility purpose.

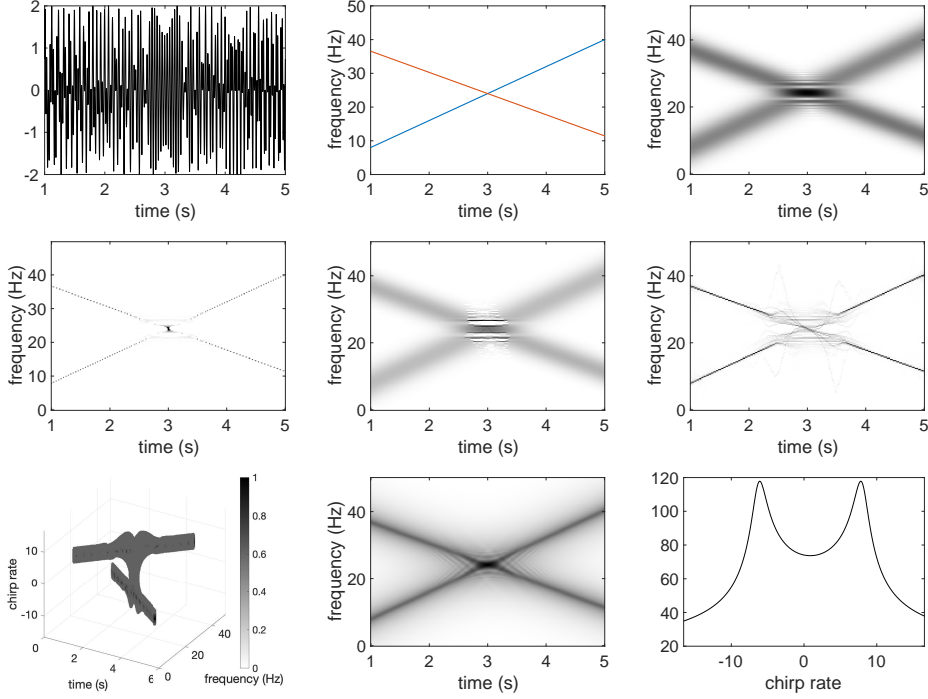


FIGURE 1. Top row, from left to right: the plot of $\Re(f_1 + f_2)$, the plot of the IFs of f_1 and f_2 , and the spectrogram. Note that their IFs have a crossing point at $(t_0, \xi_0) = (3, 24)$. All the plots are generated with the kernel $g_0 = e^{-\pi x^2}$. Second row, from left to right: the reassignment method, SST, and the 2nd-order SST. Bottom row, from left to right: the 3-dim visualization of the time-frequency-chirp rate representation $|T_f^{(g_0)}(t, \xi, \lambda)|$, the projection of $|T_f^{(g_0)}(t, \xi, \lambda)|$ onto the time-frequency plane, and the plot of $|T_f^{(g_0)}(t_0, \xi_0, \lambda)|$. For each time-frequency representation, we set all entries with the magnitude above the 99.99% percentile of all entries to be the magnitude of the 99.99% percentile.

The rest of the paper is organized as follows. In Section 2, we first introduce the chirp transform and study its properties, and then introduce the synchrosqueezed chirplet transform (SCT). We elaborate on the theoretical results of the SCT in Section 4. Finally, we provide numerical results of SCT in Section 5.

2. CHIRPLET TRANSFORM AND ITS SQUEEZING

2.1. Chirplet transform. We start our exploration by introducing the definition of the chirplet transform (CT). Denote $\mathcal{S}(\mathbb{R})$ to be the Schwartz space and $\mathcal{S}'(\mathbb{R})$ to be the tempered distribution space.

Definition 1 (Chirplet transforms (CT) [26]). The chirplet transform of a tempered distribution $f \in \mathcal{S}'(\mathbb{R})$ associated with a window function $g \in \mathcal{S}(\mathbb{R})$ at (t, ξ, λ) is defined as

$$T_f^{(g)}(t, \xi, \lambda) := \langle f(\cdot), g(\cdot - t)e^{-2\pi i\xi(\cdot - t)}e^{-\pi i\lambda(\cdot - t)^2} \rangle,$$

where $\langle \cdot, \cdot \rangle$ indicates the evaluation of a tempered distribution at a Schwartz function, $t \in \mathbb{R}$ indicates *time*, $\xi \in \mathbb{R}$ indicates *frequency* and $\lambda \in \mathbb{R}$ indicates the *chirp rate*.

In general, since g is Schwartz, $T_f^{(g)}(t, \xi, \lambda)$ is well defined at each (t, ξ, λ) , and it is a complex function on the TFC domain. Note that when f is a function, $T_f^{(g)}(t, \xi, \lambda)$ has an integration form $\int_{\mathbb{R}} f(x)g(x - t)e^{-2\pi i\xi(x - t)}e^{-\pi i\lambda(x - t)^2} dx$.

Definition 2 (Time-frequency-chirp rate representation and time-frequency representation determined by the chirplet transform). Following Definition 1, we call $|T_f^{(g)}(t, \xi, \lambda)|$ the *TFC representation* of the signal f with the window g . We define the *TF representation determined by CT* as the projection of the TFC representation onto the TF domain, denoted as $\mathfrak{T}_f^{(g)}(t, \xi)$, which is defined as

$$\mathfrak{T}_f^{(g)}(t, \xi) := \int_{-\infty}^{\infty} |T_f^{(g)}(t, \xi, \lambda)| d\lambda.$$

From the dictionary learning perspective, $T_f^{(g)}(t, \xi, \lambda)$ comes from fitting an atom with frequency ξ and chirp rate λ when the signal is centered at t and truncated by the Gaussian window.

An immediate question we would like to ask is the uncertainty principle associated with CT. We illustrate this point by evaluating CT of a pure linear chirp $f(x) = e^{2\pi i\xi_0 x + \pi i\lambda_0 x^2}$, where $\xi_0, \lambda_0 \in \mathbb{R}$, and show that we cannot simultaneously sharply localize a signal in both the time domain and chirp rate domain. By directly expanding the CT with the window $g(x) = e^{-\pi\alpha x^2}$, where $\alpha > 0$, we have

$$\begin{aligned} T_f^{(g)}(t, \xi, \lambda) &= \int e^{2\pi i\xi_0 x + \pi i\lambda_0 x^2} e^{-\pi\alpha(x-t)^2} e^{-2\pi i\xi(x-t)} e^{-\pi i\lambda(x-t)^2} dx \\ &= e^{2\pi i\xi_0 t + \pi i\lambda_0 t^2} \int e^{-\pi(\alpha - i\lambda_0 + i\lambda)x^2} e^{-2\pi i(-\xi_0 - \lambda_0 t + \xi)x} dx \\ (1) \quad &= e^{2\pi i\xi_0 t + \pi i\lambda_0 t^2} \frac{1}{\sqrt{\alpha + i(\lambda - \lambda_0)}} e^{\frac{-\pi(\xi - \xi_0 - \lambda_0 t)^2}{\alpha + i(\lambda - \lambda_0)}}, \end{aligned}$$

whose magnitude is

$$\left| T_f^{(g)}(t, \xi, \lambda) \right| = \frac{1}{\sqrt{\alpha^2 + (\lambda - \lambda_0)^2}} e^{\frac{-\pi\alpha(\xi - \xi_0 - \lambda_0 t)^2}{\alpha^2 + (\lambda - \lambda_0)^2}}.$$

Lemma 1. Take $f(x) = e^{2\pi i\xi_0 x + \pi i\lambda_0 x^2}$. For a fixed $\alpha > 0$ and $t \in \mathbb{R}$, when ξ is sufficiently close to $\xi_0 + \lambda_0 t$, $\left| T_f^{(g)}(t, \xi, \lambda) \right|$ is of order $\frac{1}{\sqrt{|\lambda - \lambda_0|}} \max_{\lambda} \left| T_f^{(g)}(t, \xi, \lambda) \right|$

Proof. Since t and $\alpha > 0$ are fixed, we can find ξ close to $\xi_0 + \lambda_0 t$ so that

$$4\pi\alpha(\xi - \xi_0 - \lambda_0 t)^2 \leq \alpha^2 + (\lambda - \lambda_0)^2$$

for any λ . Particularly, when $\lambda = \lambda_0$, $\alpha \geq 4\pi(\xi - \xi_0 - \lambda_0 t)^2$. Denote $C = C(\xi) = (\xi - \xi_0 - \lambda_0 t)^2$. Clearly, $C \leq \frac{\alpha}{4\pi}$. For the fixed t and the chosen ξ , we investigate the monotonicity of $M(\lambda) := \left| T_f^{(g)}(t, \xi, \lambda) \right|$, which is equivalent to checking the monotonicity of $\ln(M(\lambda))$:

$$\begin{aligned} \ln(M(\lambda)) &= -\frac{\pi\alpha(\xi - \xi_0 - \lambda_0 t)^2}{\alpha^2 + (\lambda - \lambda_0)^2} - \frac{1}{4} \log(\alpha^2 + (\lambda - \lambda_0)^2), \\ \frac{d\ln(M(\lambda))}{d\lambda} &= \frac{2\pi\alpha(\xi - \xi_0 - \lambda_0 t)^2(\lambda - \lambda_0)}{(\alpha^2 + (\lambda - \lambda_0)^2)^2} - \frac{\lambda - \lambda_0}{2(\alpha^2 + (\lambda - \lambda_0)^2)} \\ &= \frac{\lambda - \lambda_0}{2(\alpha^2 + (\lambda - \lambda_0)^2)} \left(\frac{4\pi\alpha(\xi - \xi_0 - \lambda_0 t)^2}{\alpha^2 + (\lambda - \lambda_0)^2} - 1 \right), \end{aligned}$$

which indicates that $\frac{d\ln(M(\lambda))}{d\lambda} \leq 0$ when $\lambda \geq \lambda_0$, and $\frac{d\ln(M(\lambda))}{d\lambda} \geq 0$ when $\lambda \leq \lambda_0$. Since $\left| T_f^{(g)}(t, \xi, \lambda_0) \right| = \frac{1}{\sqrt{\alpha}} e^{-\frac{\pi C}{\alpha}}$, when ξ is sufficiently close to $\xi_0 + \lambda_0 t$, we have $\max_{\lambda} \left| T_f^{(g)}(t, \xi, \lambda) \right| = \frac{1}{\sqrt{\alpha}} e^{-\frac{\pi C}{\alpha}}$.

Next, we solve for λ to see when the magnitude will decrease to $\frac{1}{\rho}$ of its maximum, where $\rho > 1$. The desired equality

$$\frac{1}{\sqrt[4]{\alpha^2 + (\lambda - \lambda_0)^2}} e^{-\frac{\pi\alpha C}{\alpha^2 + (\lambda - \lambda_0)^2}} = \frac{1}{\rho} \max_{\lambda} \left| T_f^{(g)}(t, \xi, \lambda) \right| = \frac{1}{\rho\sqrt{\alpha}} e^{-\frac{\pi C}{\alpha}}$$

gives

$$\frac{-4\pi\alpha C}{\alpha^2 + (\lambda - \lambda_0)^2} = \ln(\alpha^2 + (\lambda - \lambda_0)^2) - \ln(\rho^4 \alpha^2) - \frac{4\pi C}{\alpha},$$

which is equivalent to

$$\ln(\alpha^2 + (\lambda - \lambda_0)^2) + \frac{4\pi\alpha C}{\alpha^2 + (\lambda - \lambda_0)^2} = \ln(\rho^4 \alpha^2) + \frac{4\pi C}{\alpha}.$$

Let $\lambda - \lambda_0 = k\alpha$, where $k \in \mathbb{R}$ will be determined. Then the above equality becomes

$$(2) \quad \ln(k^2 + 1) + \frac{4\pi C}{(k^2 + 1)\alpha} = \ln(\rho^4) + \frac{4\pi C}{\alpha}.$$

Clearly, when $\xi = \xi_0 + \lambda_0 t$, $C = 0$ and $k = \sqrt{\rho^4 - 1}$. In general, we need to take C into account. Note that the derivative of the left hand side of (2) in terms of k satisfies

$$\partial_k \left(\ln(k^2 + 1) + \frac{4\pi C}{(k^2 + 1)\alpha} \right) = \frac{2k}{k^2 + 1} + \frac{4\pi C}{\alpha} \frac{-2k}{(k^2 + 1)^2} = \left(1 - \frac{4\pi C}{\alpha} \frac{1}{k^2 + 1} \right) \frac{2k}{k^2 + 1} > 0$$

since $\alpha \geq 4\pi C$ when ξ is close to $\xi_0 + \lambda_0 t$. So $\ln(k^2 + 1) + \frac{4\pi C}{(k^2 + 1)\alpha}$ is an increasing function of $|k|$. To solve the problem, we consider the following two cases.

- If $k^2 + 1 = \rho^4$, i.e. $|k| = \sqrt{\rho^4 - 1}$, then

$$\ln(k^2 + 1) + \frac{4\pi C}{(k^2 + 1)\alpha} = \ln(\rho^4) + \frac{4\pi C}{\rho^4 \alpha} \leq \ln(\rho^4) + \frac{4\pi C}{\alpha},$$

since $\rho > 1$, and the equality holds when $C = 0$.

- If $k^2 = e\rho^4$, where $e = \exp(1)$, i.e. $|k| = \sqrt{e}\rho^2$, then

$$\ln(k^2 + 1) + \frac{4\pi C}{(k^2 + 1)\alpha} - \ln(\rho^4) - \frac{4\pi C}{\alpha} = \ln\left(e + \frac{1}{\rho^4}\right) - \frac{4\pi C}{\alpha} \left(1 - \frac{1}{e\rho^4 + 1}\right) \geq 0,$$

since $\frac{4\pi C}{\alpha} \left(1 - \frac{1}{e\rho^4 + 1}\right) < \frac{4\pi C}{\alpha} \leq 1$.

Therefore, the λ for the magnitude decreasing to $\frac{1}{\rho}$ of its maximum lies between

$$\sqrt{\rho^4 - 1}\alpha \leq |\lambda - \lambda_0| < \sqrt{e}\rho^2\alpha.$$

Note that where both the upper and the lower bounds scale linearly with α , hence if the signal is more localized in time (α is larger), it is less localized in the chirp rate domain. Moreover, when ξ is close to $\xi_0 + \lambda_0 t$ and α is fixed, $|\lambda - \lambda_0|$ is of order ρ^2 . Thus, $\left|T_f^{(g)}(t, \xi, \lambda)\right|$ is of order $\frac{1}{\sqrt{|\lambda - \lambda_0|}} \max_{\lambda} \left|T_f^{(g)}(t, \xi, \lambda)\right|$, as is claimed. \square

This lemma indicates that for the linear chirp, the CT in the chirp rate axis decays slowly. This explains the blurring of the TFC representation shown in Figure 1.

2.2. Some properties of chirp transform. Before introducing our algorithm we discuss some properties of the general chirp transform.

Definition 3 (Chirp transforms). The chirp transform of a function $f \in L^1(\mathbb{R})$ is defined as

$$Tf(\lambda) = \int_{\mathbb{R}} f(x) e^{-\pi i \lambda x^2} dx,$$

where $\lambda \in \mathbb{R}$.

Note that the chirplet transform is nothing but a special case of the chirp transform, with $f(x)$ replaced by $f(x)g(x-t)e^{-2\pi i \xi(x-t)}$. We start by asking a basic question – since the chirp transform is similar to the Fourier transform, may we obtain those basic properties of the Fourier transform for the chirp transform? For example, is the chirp transform of a L^1 function continuous and decay like that stated in the Riemann-Lebesgue theorem? Does the chirp transform preserve the L^2 norm like the Plancherel theorem? To study these properties, we introduce some function spaces that we will use in the following propositions. We say a function $f(x) \in W_0^{1,1}(\mathbb{R})$, if $\lim_{|x| \rightarrow \infty} f(x) = 0$, and both $f(x)$ and $f'(x)$ in the weak sense are in $L^1(\mathbb{R})$; a function $f(x) \in C_0^{2n}(\mathbb{R})$, if f is $2n$ times continuously differentiable and $\lim_{|x| \rightarrow \infty} f^{(k)}(x) = 0$ for $k = 1, \dots, 2n$. Also, denote $C_c^\infty(\mathbb{R})$ to be the set of smooth functions with compact support.

We start with investigating if the magnitude of chirp transform has some decay property in terms of chirp rate. First we have

Lemma 2. For $-\infty \leq a < b \leq \infty$, we have

$$\left| \int_a^b e^{-\pi i \lambda x^2} dx \right| \leq \left(\frac{3}{\pi} + 2 \right) \lambda^{-\frac{1}{2}}.$$

Proof. We only show the case where $0 \in (a, b)$, the argument for $0 \in \mathbb{R} \setminus (a, b)$ is similar. Choose $\delta > 0$ and split the integral into

$$\int_a^{-\delta} e^{-\pi i \lambda x^2} dx + \int_{-\delta}^{\delta} e^{-\pi i \lambda x^2} dx + \int_{\delta}^b e^{-\pi i \lambda x^2} dx$$

For the first integral, integration by parts gives

$$\begin{aligned}
\left| \int_a^{-\delta} e^{-\pi i \lambda x^2} dx \right| &= \left| \int_a^{-\delta} \frac{1}{-2\pi i \lambda x} \frac{d e^{-\pi i \lambda x^2}}{dx} dx \right| \\
&\leq \left| \frac{e^{-\pi i \lambda x^2}}{2\pi \lambda x} \Big|_{x=a}^{-\delta} \right| + \left| \int_a^{-\delta} e^{-\pi i \lambda x^2} \frac{d}{dx} \left(\frac{1}{2\pi i \lambda x} \right) dx \right| \\
&\leq \frac{1}{\pi \lambda \delta} + \frac{1}{2\pi \lambda} \int_a^{-\delta} \left| \frac{d}{dx} \left(\frac{1}{x} \right) \right| dx \\
&= \frac{1}{\pi \lambda \delta} + \frac{1}{2\pi \lambda} \left| \int_a^{-\delta} \frac{d}{dx} \left(\frac{1}{x} \right) dx \right| \quad (\text{by the monotonicity of } \frac{1}{x} \text{ on } (a, -\delta)) \\
&\leq \frac{1}{\pi \lambda \delta} + \frac{1}{2\pi \lambda \delta} = \frac{3}{2\pi \lambda \delta}.
\end{aligned}$$

By the same argument, we also have

$$\left| \int_{\delta}^b e^{-\pi i \lambda x^2} dx \right| \leq \frac{3}{2\pi \lambda \delta},$$

combined with $\left| \int_{-\delta}^{\delta} e^{-\pi i \lambda x^2} dx \right| \leq 2\delta$, we have

$$\left| \int_a^b e^{-\pi i \lambda x^2} dx \right| \leq \frac{3}{\pi \lambda \delta} + 2\delta.$$

Take $\delta = \lambda^{-\frac{1}{2}}$, and we have $\left| \int_a^b e^{-\pi i \lambda x^2} dx \right| \leq \left(\frac{3}{\pi} + 2 \right) \lambda^{-\frac{1}{2}}$. \square

Proposition 1. Suppose $f(x) \in W_0^{1,1}(\mathbb{R})$, then $|Tf(\lambda)| \leq \left(\frac{3}{\pi} + 2 \right) \|f'\|_1 \lambda^{-\frac{1}{2}}$.

Proof. When $f \in C_c^\infty(\mathbb{R}) \subset W_0^{1,1}(\mathbb{R})$, by the change of variable, we have

$$Tf(\lambda) = \int f(x) \frac{d}{dx} \left(\int_{-\infty}^x e^{-\pi i \lambda t^2} dt \right) dx = - \int f'(x) \left(\int_{-\infty}^x e^{-\pi i \lambda t^2} dt \right) dx,$$

so by Lemma 2, we have

$$|Tf(\lambda)| \leq \int |f'(x)| \left| \int_{-\infty}^x e^{-\pi i \lambda t^2} dt \right| dx \leq \left(\frac{3}{\pi} + 2 \right) \lambda^{-\frac{1}{2}} \int |f'(x)| dx.$$

Since $C_c^\infty(\mathbb{R})$ is dense in $W_0^{1,1}(\mathbb{R})$, we get the proof by a direct extension argument. \square

We have several properties of the chirp transforms that are parallel to some properties of the Fourier transforms.

Proposition 2. Let $f \in L^1(\mathbb{R})$, then $Tf(\lambda)$ is uniformly continuous.

Proof. Take $\epsilon > 0$. For any $h, r > 0$, we have the following control:

$$\begin{aligned} |Tf(\lambda + h) - Tf(\lambda)| &= \left| \int f(x)(e^{-\pi i(\lambda+h)x^2} - e^{-\pi i\lambda x^2}) dx \right| \\ &\leq \int |f(x)| |e^{-\pi ihx^2} - 1| dx \\ &= \int_{|x| \leq r} |f(x)| |e^{-\pi ihx^2} - 1| dx + \int_{|x| > r} |f(x)| |e^{-\pi ihx^2} - 1| dx \\ &\leq \int_{|x| \leq r} |f(x)| \pi |h| x^2 dx + 2 \int_{|x| > r} |f(x)| dx. \end{aligned}$$

We only need to choose h and r so that $\int_{|x| > r} |f(x)| dx < \frac{\epsilon}{4}$, and $\pi |h| r^2 < \frac{\epsilon}{2\|f\|_1}$. \square

By Propositions 1 and 2, we know that the chirp transform, and hence CT, has a similar property as the Riemann-Lebesgue Theorem of the Fourier transform.

Proposition 3. For $f \in L^1(\mathbb{R})$, if $x^2 f(x) \in L^1(\mathbb{R})$, then $Tf(\lambda)$ is differentiable and

$$\frac{dTf(\lambda)}{d\lambda} = -\pi iT(x^2 f)(\lambda).$$

Proof. The proof is straightforward by applying the dominated convergence theorem. \square

Unfortunately, we do not have a norm-preserving theorem for the chirp transforms similar to the Plancherel theorem in the Fourier transforms partially due to the slow decay rate in λ . On the contrary, we show that the chirp transforms do not satisfy “most” of the weak type inequalities.

Proposition 4. The chirp transform operator T is not weak-type (p, q) , if $\frac{2q}{p} - 2q + 4 \neq 0$.

Proof. Fix $p > 1$. We show that for any $C > 0$, there exists $f \in L^p(\mathbb{R})$ and $\eta > 0$, such that

$$m(\{\lambda : |Tf(\lambda)| > \eta\}) > \frac{C \|f\|_p^q}{\eta^q},$$

where $\frac{2q}{p} - 2q + 4 \neq 0$ and m is the Lebesgue measure. Let $f_\alpha(x) = \alpha^{\frac{1}{p}} e^{-\frac{\pi \alpha^2 x^2}{p}}$, $\alpha > 0$. One can verify that $\|f_\alpha\|_p = 1$ for any $\alpha > 0$. It suffices to show that for any $C > 0$, we can always find $\alpha, \eta > 0$, such that

$$(3) \quad m(\{\lambda : |Tf_\alpha(\lambda)| > \eta\}) > \frac{C \|f_\alpha\|_p^q}{\eta^q} = \frac{C}{\eta^q}.$$

It is easy to obtain $Tf_\alpha(\lambda) = \frac{\alpha^{\frac{1}{p}}}{\sqrt{\frac{\alpha^2}{p} + i\lambda}}$, so $|Tf_\alpha(\lambda)| = \frac{\alpha^{\frac{1}{p}}}{\sqrt{\frac{\alpha^4}{p^2} + \lambda^2}}$. By solving the inequality $\frac{\alpha^{\frac{1}{p}}}{\sqrt{\frac{\alpha^4}{p^2} + \lambda^2}} > \eta$, we have

$$(4) \quad m(\{\lambda : |Tf_\alpha(\lambda)| > \eta\}) = 2\sqrt{\frac{\alpha^{\frac{4}{p}}}{\eta^4} - \frac{\alpha^4}{p^2}},$$

for $\frac{\alpha^{\frac{4}{p}}}{\eta^4} - \frac{\alpha^4}{p^2} > 0$; otherwise the measure is zero. Note that the condition $\frac{\alpha^{\frac{4}{p}}}{\eta^4} - \frac{\alpha^4}{p^2} > 0$ gives $\eta < \alpha^{\frac{1}{p}-1} p^{\frac{1}{2}}$. Select $\eta = \frac{1}{2} \alpha^{\frac{1}{p}-1} p^{\frac{1}{2}}$. We now determine α . With (4) and the selected η , (3) becomes

$$2 \sqrt{\frac{\alpha^{\frac{4}{p}}}{(\frac{1}{2} \alpha^{\frac{1}{p}-1} p^{\frac{1}{2}})^4} - \frac{\alpha^4}{p^2}} > \frac{C}{(\frac{1}{2} \alpha^{\frac{1}{p}-1} p^{\frac{1}{2}})^q}.$$

Simplifying this inequality gives us

$$\alpha^{\frac{2q}{p}-2q+4} > \frac{2^{2q-2}}{15} C^2 p^{2-q}.$$

Therefore, if $\frac{2q}{p} - 2q + 4 > 0$, we can set α to be sufficiently large, so that the left hand side is larger than the right hand side; if $\frac{2q}{p} - 2q + 4 < 0$, we can set α to be sufficiently small. We thus finish the claim. \square

Corollary 1. The chirp transform operator T is not weak-type $(2, 2)$.

We next show that the decay rate of $Tf(\lambda)$ is related to the vanishing order of f at the origin.

Proposition 5. Suppose $f(x) \in C_0^{2n}(\mathbb{R})$, $n \geq 1$ and $f \in L^1(\mathbb{R})$. If we assume that $f(0) = f'(0) = \dots = f^{(2n-2)}(0) = 0$ and $f^{(2n)}(0) \neq 0$, then

$$|Tf(\lambda)| \leq C \lambda^{-\frac{2n+1}{3}},$$

for some constant $C > 0$ and C depends on n and f .

Proof. Fix $\lambda > 0$. Let D be a differential operator such that $Df := -\frac{1}{2\pi i \lambda} \frac{df}{dx}$, and \tilde{D} such that $\tilde{D}f := \frac{1}{2\pi i \lambda} \frac{d}{dx}(\frac{f}{x})$. First, if f satisfies the above conditions and is zero in $(-\epsilon, \epsilon)$ for some $\epsilon > 0$, since $D^k(e^{-\pi i \lambda x^2}) = e^{-\pi i \lambda x^2}$ for any k and $x \neq 0$, we have

$$\begin{aligned} Tf(\lambda) &= \int_{\mathbb{R} \setminus (-\epsilon, \epsilon)} f(x) e^{-\pi i \lambda x^2} dx \\ &= \int_{\mathbb{R} \setminus (-\epsilon, \epsilon)} f(x) D^{2n}(e^{-\pi i \lambda x^2}) dx = \int_{\mathbb{R} \setminus (-\epsilon, \epsilon)} \tilde{D}^{2n}(f) e^{-\pi i \lambda x^2} dx. \end{aligned}$$

One can easily show by induction on n together with the boundedness of the derivatives of f that $|Tf(\lambda)| \leq C \lambda^{-2n} \epsilon^{-(4n-1)}$ for some $C > 0$ that depends on n and f .

Then we prove the statement of the proposition. Suppose for some $\epsilon > 0$, we can write f in its Taylor expansion:

$$\begin{aligned} f(x) &= f(0) + f'(0)x + \dots + \frac{f^{(2n-1)}(0)}{(2n-1)!} x^{2n-1} + \frac{f^{(2n)}(\xi(x))}{(2n)!} x^{2n} \\ &= f'(0)x + \dots + \frac{f^{(2n-3)}(0)}{(2n-3)!} x^{2n-3} + \frac{f^{(2n-1)}(0)}{(2n-1)!} x^{2n-1} + \frac{f^{(2n)}(\xi(x))}{(2n)!} x^{2n} \end{aligned}$$

for $|x| < 2\epsilon$, and $\xi(x)$ is some number between 0 and x . Suppose $\psi(x) \in C_c^\infty(\mathbb{R})$ with $\psi(x) = 1$ for $|x| \leq 1$, and $\psi(x) = 0$ for $|x| \geq 2$, and we also assume ψ is even. Then we can decompose f into $f(x) = f(x)\psi(\frac{x}{\epsilon}) + f(x)(1 - \psi(\frac{x}{\epsilon}))$. From the first part of the proof, we know that $|T((1 - \psi(\frac{x}{\epsilon}))f)(\lambda)| \leq C \lambda^{-2n} \epsilon^{-(4n-1)}$. On the

other hand, $T(x^k \psi(\frac{x}{\epsilon}))(\lambda) = 0$ for odd k by symmetry. What remains is controlling $\frac{f^{(2n)}(\xi(x))}{(2n)!} x^{2n} \psi(\frac{x}{\epsilon})$. By the boundedness of $f^{(2n)}(x)$, we have

$$\left| T \left(\frac{f^{(2n)}(\xi(x))}{(2n)!} x^{2n} \psi\left(\frac{x}{\epsilon}\right) \right) (\lambda) \right| \leq C \int_{|x| \leq 2\epsilon} x^{2n} dx \leq C \epsilon^{2n+1},$$

where $C > 0$ depends on n and f . Combining these estimations, we have

$$|Tf(\lambda)| \leq C(\lambda^{-2n} \epsilon^{-(4n-1)} + \epsilon^{2n+1}).$$

If we select $\epsilon = \lambda^{-\frac{1}{3}}$, we have

$$|Tf(\lambda)| \leq C \lambda^{-\frac{2n+1}{3}}$$

□

3. PROPOSED ALGORITHM – SYNCHROSQUEEZED CHIRPLET TRANSFORM

The above result led us to consider if it is possible to sharpen the TFC representation by some idea similar to the reassignment technique, like synchrosqueezing [12], used to handle the uncertainty principle of the linear-type TF analysis algorithms. Indeed, we ask if it is possible to manipulate the phase information in CT so that the TFC representation can be sharpened. Below we introduce this idea with a linear chirp $f(x) = e^{2\pi i \xi_0 x + \pi i \lambda_0 x^2}$, where λ_0 is allowed to be large. Note that the idea of the original SST might not be suitable for our purpose due to the non-trivial chirp rate. Instead, we need to consider the higher order phase information, like that considered in the second order SST [28, 3], to handle the possibly non trivial chirp rate. Take any window function $g(x)$ in the Schwartz space. Since

$$\begin{aligned} T_f^{(g)}(t, \xi, \lambda) &= \int e^{2\pi i \xi_0 x + \pi i \lambda_0 x^2} g(x-t) e^{-2\pi i \xi(x-t)} e^{-\pi i \lambda(x-t)^2} dx \\ &= e^{2\pi i \xi_0 t + \pi i \lambda_0 t^2} \int g(x) e^{-\pi i(\lambda - \lambda_0)x^2} e^{-2\pi i(\xi - \xi_0 - \lambda_0 t)x} dx \end{aligned}$$

by a direct expansion we have

$$(5) \quad \partial_t T_f^{(g)} = (2\pi i \xi_0 + 2\pi i \lambda_0 t) T_f^{(g)} + 2\pi i \lambda_0 T_f^{(xg)}$$

and

$$(6) \quad \partial_\xi T_f^{(g)} = -2\pi i T_f^{(xg)}.$$

Then from (5) and (6) we have

$$\partial_t \left(\frac{\partial_t T_f^{(g)}}{T_f^{(g)}} \right) = 2\pi i \lambda_0 \left(1 + \partial_t \left(\frac{T_f^{(xg)}}{T_f^{(g)}} \right) \right) = \lambda_0 \left(2\pi i - \partial_t \left(\frac{\partial_\xi T_f^{(g)}}{T_f^{(g)}} \right) \right),$$

so

$$\lambda_0 = \frac{\partial_t \left(\frac{\partial_t T_f^{(g)}}{T_f^{(g)}} \right)}{2\pi i - \partial_t \left(\frac{\partial_\xi T_f^{(g)}}{T_f^{(g)}} \right)}.$$

In addition, from (5) we can solve for the frequency,

$$\xi_0 + \lambda_0 t = \frac{\partial_t T_f^{(g)} - 2\pi i \lambda_0 T_f^{(xg)}}{2\pi i T_f^{(g)}}.$$

The above equalities motivate us to propose the reassignment operators:

$$\begin{aligned} \mu_f^{(g)}(t, \xi, \lambda) &:= \frac{\partial_t \left(\frac{\partial_t T_f^{(g)}}{T_f^{(g)}} \right)}{2\pi i - \partial_t \left(\frac{\partial_\xi T_f^{(g)}}{T_f^{(g)}} \right)}, \\ \omega_f^{(g)}(t, \xi, \lambda) &:= \frac{\partial_t T_f^{(g)} - 2\pi i \mu_f^{(g)}(t, \xi, \lambda) T_f^{(xg)}}{2\pi i T_f^{(g)}} = \frac{\partial_t T_f^{(g)} - \mu_f^{(g)}(t, \xi, \lambda) \partial_\xi T_f^{(g)}}{2\pi i T_f^{(g)}}. \end{aligned}$$

We can calculate the partial derivatives, and the expression for $\mu_f^{(g)}$ becomes

$$\mu_f^{(g)}(t, \xi, \lambda) = \frac{T_f^{(g)} \partial_{tt}^2 T_f^{(g)} - (\partial_t T_f^{(g)})^2}{2\pi i (T_f^{(g)})^2 + 2\pi i (T_f^{(g)}) \partial_t T_f^{(xg)} - T_f^{(xg)} \partial_t T_f^{(g)}}.$$

The above calculations lead us to the following definition.

Definition 4 (Synchrosqueezed chirplet transform). Take $f \in \mathcal{S}'(\mathbb{R})$ and $g \in \mathcal{S}(\mathbb{R})$ as the window. For a small $\alpha > 0$, define the *synchrosqueezed chirplet transform* (SCT) with *resolution* α as

$$S_f^{(g, \alpha)}(t, \xi, \lambda) := \iint_{\mathbb{R}^2} T_f^{(g)}(t, \eta, \gamma) h_\alpha(\xi - \omega_f^{(g)}(t, \eta, \gamma)) h_\alpha(\lambda - \mu_f^{(g)}(t, \eta, \gamma)) d\eta d\gamma,$$

where h_α is an ‘‘approximate δ -function’’ (i.e. h is smooth and decays fast with $\int h(x) dx = 1$, so that $h_\alpha(t) := \frac{1}{\alpha} h(\frac{t}{\alpha})$ tends weakly to the delta measure δ as $\alpha \rightarrow 0$). Similar to $\mathfrak{T}_f^{(g)}(t, \xi)$, we define the TF representation associated with SCT via projecting the TFC representation onto the TF domain:

$$\mathfrak{S}_f^{(g, \alpha)}(t, \xi) = \int_{-\infty}^{\infty} |S_f^{(g, \alpha)}(t, \xi, \lambda)| d\lambda.$$

A main practical concern of SCT is numerical stability, since differentiations in the calculation of $\mu_f^{(g)}$ and $\omega_f^{(g)}$ are numerically unstable. This concern is numerically handled by noting that $\omega_f^{(g)}$ and $\mu_f^{(g)}$ can be calculated directly with different window functions without any differentiation. Indeed, note that by a direct expansion, we have

$$\partial_t T_f^{(g)} = -T_f^{(g')} + 2\pi i \xi T_f^{(g)} + 2\pi i \lambda T_f^{(xg)},$$

and

$$\begin{aligned} \partial_{tt}^2 T_f^{(g)} &= T_f^{(g'')} - 4\pi i \xi T_f^{(g')} - 2\pi i \lambda T_f^{(xg')} + (2\pi i \xi)^2 T_f^{(g)} + 2(2\pi i \xi)(2\pi i \lambda) T_f^{(xg)} \\ &\quad - 2\pi i \lambda T_f^{(g+xg')} + (2\pi i \lambda)^2 T_f^{(x^2g)}. \end{aligned}$$

Therefore, we have

$$\mu_f^{(g)}(t, \xi, \lambda) = \frac{T_f^{(g)} \partial_{tt}^2 T_f^{(g)} - (\partial_t T_f^{(g)})^2}{2\pi i (T_f^{(g)})^2 + 2\pi i (T_f^{(g)}) \partial_t T_f^{(xg)} - T_f^{(xg)} \partial_t T_f^{(g)}} = \frac{A}{B},$$

where $A := T_f^{(g)}T_f^{(g'')} - 4\pi i\lambda T_f^{(g)}T_f^{(xg')} - 2\pi i\lambda(T_f^{(g)})^2 + (2\pi i\lambda)^2 T_f^{(g)}T_f^{(x^2g)} - (T_f^{(g')})^2 - (2\pi i\lambda)^2(T_f^{(xg)})^2 + 4\pi i\lambda T_f^{(g')}T_f^{(xg)}$ and $B := -2\pi i T_f^{(g)}T_f^{(xg')} + (2\pi i)^2\lambda T_f^{(g)}T_f^{(x^2g)} + 2\pi i T_f^{(xg)}T_f^{(g')} - (2\pi i)^2\lambda(T_f^{(xg)})^2$ and

$$\omega_f^{(g)}(t, \xi, \lambda) = \frac{\partial_t T_f^{(g)} - 2\pi i\mu_f^{(g)}T_f^{(xg)}}{2\pi i T_f^{(g)}} = \xi + \frac{-T_f^{(g')} + 2\pi i\lambda T_f^{(xg)} - 2\pi i\mu_f^{(g)}T_f^{(xg)}}{2\pi i T_f^{(g)}}.$$

The numerical implementation of SCT will be detailed below.

Remark 1. We shall compare SCT with SST and its 2nd-order variation. Recall that the Short-time Fourier transform (STFT) of a tempered distribution $f \in \mathcal{S}'(\mathbb{R})$ associated with a window function $g \in \mathcal{S}(\mathbb{R})$ at (t, ξ) is defined as

$$W_f^{(g)}(t, \xi) := \langle f(\cdot), g(\cdot - t)e^{-2\pi i\xi(\cdot - t)} \rangle,$$

where $\langle \cdot, \cdot \rangle$ indicates the evaluation of a tempered distribution at a Schwartz function, $t \in \mathbb{R}$ indicates *time*, $\xi \in \mathbb{R}$ indicates *frequency*. With the same h_α as in the definition of SCT, the STFT-based SST of $f \in \mathcal{S}'(\mathbb{R})$ with $g \in \mathcal{S}(\mathbb{R})$ and *resolution* α is then defined as [34]

$$S_f^{1,(g,\alpha)}(t, \xi) := \int_{\mathbb{R}} W_f^{(g)}(t, \eta) h_\alpha(\xi - \omega_f^{1,(g)}(t, \eta)) d\eta,$$

where

$$\omega_f^{1,(g)}(t, \xi) = \frac{\partial_t W_f^{(g)}(t, \xi)}{2\pi i W_f^{(g)}(t, \xi)};$$

the STFT-based 2nd-order SST of $f \in \mathcal{S}'(\mathbb{R})$ with $g \in \mathcal{S}(\mathbb{R})$ and *resolution* α is defined as [3]

$$S_f^{2,(g,\alpha)}(t, \xi) := \int_{\mathbb{R}} W_f^{(g)}(t, \eta) h_\alpha(\xi - \omega_f^{2,(g)}(t, \eta)) d\eta,$$

where

$$\omega_f^{2,(g)}(t, \xi) = \omega_f^{1,(g)}(t, \xi) + \tilde{q}_f(t, \xi)(t - \tilde{t}_f(t, \xi)),$$

and $\tilde{t}_f(t, \xi)$ and $\tilde{q}_f(t, \xi)$ are defined as

$$\tilde{t}_f(t, \xi) := t - \frac{\partial_\xi W_f^{(g)}(t, \xi)}{2\pi i W_f^{(g)}(t, \xi)}, \quad \tilde{q}_f(t, \xi) := \frac{\partial_t \left(\frac{\partial_t W_f^{(g)}(t, \xi)}{W_f^{(g)}(t, \xi)} \right)}{2\pi i - \partial_t \left(\frac{\partial_\xi W_f^{(g)}(t, \xi)}{W_f^{(g)}(t, \xi)} \right)}.$$

In short, the SST reassigns the TF content based on the first order Taylor expansion of the phase function, and the 2nd-order SST approximates the phase function by the second order Taylor expansion, and we can view the 2nd-order SST as a special case of SCT in which the chirp rate is fixed and set to be zero.

At the first glance, the behavior of $S_f^{(g,\alpha)}(t, \xi, \lambda)$ might not be clear even if f is a function. To better understand its properties, and design algorithms to solve the challenge of crossover IFs, we consider the following model.

Definition 5 (*Intrinsic chirp type function*). Fix $\epsilon > 0$. A function $f : \mathbb{R} \rightarrow \mathbb{C}$ is said to be of the ϵ -intrinsic chirp type (ϵ -ICT) if $f(x) = A(x)e^{2\pi i\phi(x)}$ with A and ϕ having the following properties:

$$\begin{aligned} A &\in C^1(\mathbb{R}) \cap L^\infty(\mathbb{R}), \quad \phi \in C^3(\mathbb{R}), \\ \inf_{x \in \mathbb{R}} \phi'(x) &> 0, \quad \sup_{x \in \mathbb{R}} \phi'(x) < \infty, \\ A(x) > 0, \quad |A'(x)|, |A''(x)|, |\phi'''(x)| &\leq \epsilon |\phi'(x)|, \quad \forall x \in \mathbb{R}, \end{aligned}$$

By definition, an ϵ -ICT function is an oscillatory function that is locally close to a linear chirp function, where the closeness is quantified by ϵ . In addition to the chirp rate variation, the AM variations are both controlled by the IF.

Definition 6 (*Superposition of well-separated ϵ -ICT components*). A function $f : \mathbb{R} \rightarrow \mathbb{C}$ is said to be in the space $\mathcal{A}_{\epsilon, \Delta}$ of superpositions of well-separated ϵ -ICT functions, and with separation $\Delta > 0$, if there exists a finite K , such that

$$f(x) = \sum_{k=1}^K f_k(x) = \sum_{k=1}^K A_k(x) e^{2\pi i\phi_k(x)},$$

where each f_k is an ϵ -ICT function, and their respective phase functions ϕ_k satisfy

$$|\phi'_k(t) - \phi'_l(t)| + |\phi''_k(t) - \phi''_l(t)| \geq 2\Delta.$$

To describe the main property of SCT, for a Schwartz function g , we define

$$\check{g}(\xi, \lambda) := \int g(x) e^{-2\pi i\xi x} e^{-\pi i\lambda x^2} dx.$$

Theorem 1. Suppose that $f \in \mathcal{A}_{\epsilon, \Delta}$, and pick a window function $g \in \mathcal{S}(\mathbb{R})$ that satisfies $|(x^n g)\check{g}(\xi, \lambda)| \leq \frac{\sqrt{\Delta} D_n \epsilon}{\sqrt{|\xi| + |\lambda|}}$ for some $D_n > 0$, $n = 0, 1, 2$. Let $\tilde{\epsilon} = \epsilon^{\frac{1}{6}}$. Then, provided ϵ (and thus also $\tilde{\epsilon}$) is sufficiently small, the following hold:

- If $(t, \xi, \lambda) \notin Z_k$ for any $k \in \{1, \dots, K\}$, where
- $$(7) \quad Z_k := \{(t, \xi, \lambda) : |\xi - \phi'_k(t)| + |\lambda - \phi''_k(t)| < \Delta\},$$
- then $|T_f^{(g)}(t, \xi, \lambda)| \leq \tilde{\epsilon}$.
- For each tuple $(t, \xi, \lambda) \in Z_k$ such that $|T_f^{(g)}(t, \xi, \lambda)| > \tilde{\epsilon}$ and $2\pi \left| 1 + \partial_t \left(\frac{T_f^{(xg)}(t, \xi, \lambda)}{T_f^{(g)}(t, \xi, \lambda)} \right) \right| > \tilde{\epsilon}$, we have
- $$(8) \quad \left| \omega_f^{(g)}(t, \xi, \lambda) - \phi'_k(t) \right| \leq \tilde{\epsilon} \quad \text{and} \quad \left| \mu_f^{(g)}(t, \xi, \lambda) - \phi''_k(t) \right| \leq \tilde{\epsilon}.$$

The proof of Theorem 1 relies on a number of standard estimates like those in [3], which is postponed to Section A.

3.1. Window effect on SCT. The slow decay of CT shown in Lemma 1 motivated us to consider SCT. It is a natural question to ask if it is possible to “speed up” the decay rate by considering a different window? As is considered in the widely applied multitaper technique [31] and its generalization [13], we know that different windows, particularly the Hermite windows that are widely used in practice, may provide information of the signal from different aspects. Inspired by the Hermite windows and Proposition 5, we consider windows that have higher vanishing order at the origin. The first result is the following corollary that comes from Proposition 5.

Corollary 2. Suppose $f(x) \in C^{2n}(\mathbb{R}) \cap \mathcal{S}'(\mathbb{R})$, $n \geq 1$ and $f \in L^1(\mathbb{R})$. If $g(x) = x^{2n}e^{-\pi\alpha x^2}$, for any t and ξ , we have

$$\left| T_f^{(g)}(t, \xi, \lambda) \right| \leq C\lambda^{-\frac{2n+1}{3}},$$

for some constant $C > 0$, where C depends on n and f .

This result shows that the higher order of the kernel vanishing at 0, the faster decay the CT is in the chirp rate axis. This is intuitively correct since at time 0, the chirp component $e^{i\pi\lambda t^2}$ does not oscillate at all near 0. Thus, if the kernel does not vanish near or at 0, the integration against $e^{i\pi\lambda t^2}$ does not vanish. See Proposition 5 for details. Now, we provide an analysis of how the windows that vanish at the origin affect the concentration of the SCT of a two-component signal in the chirp rate direction, particularly at the time that the crossover IF happens.

Proposition 6. Suppose $f(x) = f_1(x) + f_2(x)$, where $f_1(x) = e^{2\pi i\xi_1 x + \pi i\lambda_1 x^2}$ and $f_2(x) = e^{2\pi i\xi_2 x + \pi i\lambda_2 x^2}$, and $\xi_1, \xi_2, \lambda_1, \lambda_2 \in \mathbb{R}$, $\lambda_1 \neq \lambda_2$. We also assume that at time t_0 , the IFs of f_1 and f_2 intersect; that is, $\bar{\xi} := \xi_1 + \lambda_1 t_0 = \xi_2 + \lambda_2 t_0$. The window function is $g(x) = x^n e^{-\pi\alpha x^2}$, where $\alpha > 0$ and n is a nonnegative integer. Then there exists a constant c_α which depends only on α , such that if λ is closer to λ_1 , i.e. $|\lambda - \lambda_1| < |\lambda - \lambda_2|$, we have

$$\left| \mu_f^{(g)}(t_0, \bar{\xi}, \lambda) - \lambda_1 \right| \leq \begin{cases} c_\alpha \left(\frac{\alpha^2 + (\lambda - \lambda_1)^2}{\alpha^2 + (\lambda - \lambda_2)^2} \right)^{\frac{n+1}{4}}, & \text{if } n \text{ is even;} \\ c_\alpha \left(\frac{\alpha^2 + (\lambda - \lambda_1)^2}{\alpha^2 + (\lambda - \lambda_2)^2} \right)^{\frac{n+2}{4}}, & \text{if } n \text{ is odd.} \end{cases}$$

Proof. We have already computed that for $j = 1, 2$

$$T_{f_j}^{(e^{-\pi\alpha x^2})}(t, \xi, \lambda) = e^{2\pi i\xi_j t + \pi i\lambda_j t^2} \frac{1}{\sqrt{\alpha + i(\lambda - \lambda_j)}} e^{\frac{-\pi(\xi - \xi_j - \lambda_j t)^2}{\alpha + i(\lambda - \lambda_j)}},$$

and we know from (6) that

$$\partial_\xi T_{f_j}^{(e^{-\pi\alpha x^2})}(t, \xi, \lambda) = -2\pi i T_{f_j}^{(xe^{-\pi\alpha x^2})}(t, \xi, \lambda).$$

Therefore,

$$\begin{aligned} T_{f_j}^{(g)}(t, \xi, \lambda) &= \left(\frac{-1}{2\pi i} \right)^n e^{2\pi i\xi_j t + \pi i\lambda_j t^2} \frac{1}{\sqrt{\alpha + i(\lambda - \lambda_j)}} \partial_\xi^n \left(e^{\frac{-\pi(\xi - \xi_j - \lambda_j t)^2}{\alpha + i(\lambda - \lambda_j)}} \right) \\ &= \left(\frac{-1}{2\pi i} \right)^n e^{2\pi i\xi_j t + \pi i\lambda_j t^2} \frac{1}{\sqrt{\alpha + i(\lambda - \lambda_j)}} e^{\frac{-\pi(\xi - \xi_j - \lambda_j t)^2}{\alpha + i(\lambda - \lambda_j)}} P_{n,j}(\xi - \xi_j - \lambda_j t), \end{aligned}$$

where $P_{n,i}(x)$ is a Hermite-like polynomial, and contains only even powers of x if n is even; or contains only odd powers of x if n is odd. We proceed with $g(x) = x^{2n}e^{-\pi\alpha x^2}$ for $n \geq 0$, and omit the computation for $g(x) = x^{2n+1}e^{-\pi\alpha x^2}$ which would be similar. Let us compute the reassignment rule $\mu_f^{(g)}(t_0, \xi_0, \lambda)$. First we have for $j = 1, 2$

$$\partial_t T_{f_j}^{(g)} = (2\pi i\xi_j + 2\pi i\lambda_j t + \frac{2\pi\lambda_j(\xi - \xi_j - \lambda_j t)}{\alpha + i(\lambda - \lambda_j)}) T_{f_j}^{(g)} + T_{f_j}^{(g)} \frac{\partial_t P_{2n,j}(\xi - \xi_j - \lambda_j t)}{P_{2n,j}(\xi - \xi_j - \lambda_j t)}.$$

To simplify the calculation, we denote

$$A(t, \xi, \lambda) := T_{f_1}^{(g)}(t, \xi, \lambda), \quad B(t, \xi, \lambda) := T_{f_2}^{(g)}(t, \xi, \lambda);$$

$$C_j(t, \xi, \lambda) := 2\pi i \xi_j + 2\pi i \lambda_j t + \frac{2\pi \lambda_j (\xi - \xi_j - \lambda_j t)}{\alpha + i(\lambda - \lambda_j)}, \quad j = 1, 2;$$

$$D_j(t, \xi, \lambda) := \partial_t C_j = 2\pi i \lambda_j - \frac{2\pi \lambda_j^2}{\alpha + i(\lambda - \lambda_j)}, \quad j = 1, 2;$$

$$E_j(t, \xi, \lambda) := \frac{-2\pi(\xi - \xi_j - \lambda_j t)}{\alpha + i(\lambda - \lambda_j)}, \quad j = 1, 2;$$

$$F_j(t, \xi, \lambda) := \partial_t E_j = \frac{2\pi \lambda_j}{\alpha + i(\lambda - \lambda_j)}, \quad j = 1, 2;$$

$$Q_j(t, \xi, \lambda) := \frac{\partial_t P_{2n,j}(\xi - \xi_j - \lambda_j t)}{P_{2n,j}(\xi - \xi_j - \lambda_j t)}, \quad j = 1, 2;$$

$$\tilde{Q}_j(t, \xi, \lambda) := \frac{\partial_\xi P_{2n,j}(\xi - \xi_j - \lambda_j t)}{P_{2n,j}(\xi - \xi_j - \lambda_j t)}, \quad j = 1, 2;$$

$$Z_j(t, \xi, \lambda) := \partial_t Q_j, \quad j = 1, 2; \quad \tilde{Z}_j(t, \xi, \lambda) := \partial_t \tilde{Q}_j, \quad j = 1, 2.$$

With these notations, we have

$$\partial_t T_f^{(g)} = AC_1 + AQ_1 + BC_2 + BQ_2,$$

and

$$\begin{aligned} & T_f^{(g)} \partial_{tt} T_f^{(g)} - (\partial_t T_f^{(g)})^2 \\ &= (AC_1^2 + 2AC_1Q_1 + AQ_1^2 + AD_1 + AZ_1 + BC_2^2 + 2BC_2Q_2 + BQ_2^2 + BD_2 + BZ_2)(A + B) \\ & \quad - (AC_1 + AQ_1 + BC_2 + BQ_2)^2. \end{aligned}$$

At $(t_0, \bar{\xi}, \lambda)$, since $\partial_t P_{2n,i}(\xi - \xi_i - \lambda_i t)$ is a polynomial with only odd powers of $\xi - \xi_i - \lambda_i t$, so $Q_i(t_0, \bar{\xi}, \lambda) = 0$ for any $\lambda \in \mathbb{R}$ and $i = 1, 2$; also $C_1(t_0, \bar{\xi}, \lambda) - C_2(t_0, \bar{\xi}, \lambda) = 0$. So at $(t_0, \bar{\xi}, \lambda)$,

$$\begin{aligned} & T_f^{(g)} \partial_{tt} T_f^{(g)} - (\partial_t T_f^{(g)})^2 \\ &= (AC_1^2 + AD_1 + AZ_1 + BC_2^2 + BD_2 + BZ_2)(A + B) - (AC_1 + BC_2)^2 \\ &= (AD_1 + AZ_1 + BD_2 + BZ_2)(A + B) + AB(C_1 - C_2)^2 \\ &= (A + B)(AD_1 + AZ_1 + BD_2 + BZ_2). \end{aligned}$$

Then we have for $j = 1, 2$

$$\partial_\xi T_{f_j}^{(g)} = \left(\frac{-2\pi(\xi - \xi_j - \lambda_j t)}{\alpha + i(\lambda - \lambda_j)} \right) T_{f_j}^{(g)} + T_{f_j}^{(g)} \frac{\partial_\xi P_{2n,j}(\xi - \xi_j - \lambda_j t)}{P_{2n,j}(\xi - \xi_j - \lambda_j t)}.$$

So

$$\partial_\xi T_f^{(g)} = AE_1 + A\tilde{Q}_1 + BE_2 + B\tilde{Q}_2,$$

and

$$\begin{aligned} & \partial_{t\xi}^2 T_f^{(g)} = \partial_t \partial_\xi T_f^{(g)} \\ &= (AC_1 + AQ_1)E_1 + AF_1 + (AC_1 + AQ_1)\tilde{Q}_1 + A\tilde{Z}_1 + (BC_2 + BQ_2)E_2 + BF_2 \\ & \quad + (BC_2 + BQ_2)\tilde{Q}_2 + B\tilde{Z}_2. \end{aligned}$$

Similar to Q_i , at $(t_0, \bar{\xi}, \lambda)$, we have $\tilde{Q}_i(t_0, \bar{\xi}, \lambda) = 0$ for any $\lambda \in \mathbb{R}$ and $i = 1, 2$; moreover we have $E_i(t_0, \bar{\xi}, \lambda) = 0$, hence $\partial_\xi T_f^{(g)}(t_0, \bar{\xi}, \lambda) = 0$; and it is easy to check that $Z_i(t_0, \bar{\xi}, \lambda) = -\lambda_i \tilde{Z}_i(t_0, \bar{\xi}, \lambda)$. Therefore, we have at $(t_0, \bar{\xi}, \lambda)$

$$T_f^{(g)} \partial_{t\xi}^2 T_f^{(g)} - \partial_\xi T_f^{(g)} \partial_t T_f^{(g)} = (A + B)(AF_1 + A\tilde{Z}_1 + BF_2 + B\tilde{Z}_2).$$

As a result, at $(t_0, \bar{\xi}, \lambda)$, we have

$$\begin{aligned} \left| \mu_f^{(g)}(t_0, \bar{\xi}, \lambda) - \lambda_1 \right| &= \left| \frac{\partial_t \left(\frac{\partial_t T_f^{(g)}}{T_f^{(g)}} \right)}{2\pi i - \partial_t \left(\frac{\partial_\xi T_f^{(g)}}{T_f^{(g)}} \right)} - \lambda_1 \right| \\ &= \left| \frac{T_f^{(g)} \partial_{tt} T_f^{(g)} - (\partial_t T_f^{(g)})^2}{2\pi i (T_f^{(g)})^2 - (T_f^{(g)} \partial_{t\xi}^2 T_f^{(g)} - \partial_\xi T_f^{(g)} \partial_t T_f^{(g)})} - \lambda_1 \right| \\ &= \left| \frac{AD_1 + AZ_1 + BD_2 + BZ_2}{2\pi i(A + B) - (AF_1 + A\tilde{Z}_1 + BF_2 + B\tilde{Z}_2)} - \lambda_1 \right| \\ &= \left| \frac{D_1 + Z_1 + \frac{B}{A}(D_2 + Z_2)}{(2\pi i - F_1 - \tilde{Z}_1) + \frac{B}{A}(2\pi i - F_2 - \tilde{Z}_2)} - \frac{D_1 + Z_1}{2\pi i - F_1 - \tilde{Z}_1} \right| \\ &= \left| \frac{B}{A} \right| \left| \frac{(D_2 + Z_2)(2\pi i - F_1 - \tilde{Z}_1) - (D_1 + Z_1)(2\pi i - F_2 - \tilde{Z}_2)}{(2\pi i - F_1 - \tilde{Z}_1) \left[(2\pi i - F_1 - \tilde{Z}_1) + \frac{B}{A}(2\pi i - F_2 - \tilde{Z}_2) \right]} \right| \end{aligned}$$

since $\frac{D_1 + Z_1}{2\pi i - F_1 - \tilde{Z}_1} = \lambda_1$. One can verify that the constant term in $P_{2n,j}(\xi - \xi_j - \lambda_j t)$ is $\frac{c_{2n}}{(\alpha + i(\lambda - \lambda_j))^n}$ for some $c_{2n} \in \mathbb{R}$ and $j = 1, 2$. Therefore at $(t_0, \bar{\xi}, \lambda)$, for the first term, we have

$$\left| \frac{B}{A} \right| = \left(\frac{\alpha^2 + (\lambda - \lambda_1)^2}{\alpha^2 + (\lambda - \lambda_2)^2} \right)^{\frac{1}{4} + \frac{n}{2}};$$

and the second term $\left| \frac{(D_2 + Z_2)(2\pi i - F_1 - \tilde{Z}_1) - (D_1 + Z_1)(2\pi i - F_2 - \tilde{Z}_2)}{(2\pi i - F_1 - \tilde{Z}_1) \left[(2\pi i - F_1 - \tilde{Z}_1) + \frac{B}{A}(2\pi i - F_2 - \tilde{Z}_2) \right]} \right|$ is uniformly bounded in $2n$ for fixed α , since only magnitudes of Z_i and \tilde{Z}_i grow with $2n$, and in the numerator $-Z_2 \tilde{Z}_1 + Z_1 \tilde{Z}_2 = 0$. Hence $\left| \mu_f^{(g)}(t_0, \bar{\xi}, \lambda) - \lambda_1 \right| \leq c_\alpha \left(\frac{\alpha^2 + (\lambda - \lambda_1)^2}{\alpha^2 + (\lambda - \lambda_2)^2} \right)^{\frac{1}{4} + \frac{n}{2}}$, where c_α only depends on α . \square

3.2. Reconstruction. A common mission in TF analysis is reconstructing the constituent components from the recorded signal. In the SST setup, provided the window function g does not vanish at the origin, the reconstruction $\tilde{f}_k(x)$ of the k -th component $f_k(x)$ of the original signal $f(x) = \sum_{i=1}^K f_i(x)$ is

$$\tilde{f}(x) = \frac{1}{g(0)} \int_{|\xi - \phi'_k(x)| \leq \delta} S_f^{1,(g,\alpha)}(t, \xi) d\xi,$$

for some small $\delta > 0$; replacing $S_f^{1,(g,\alpha)}(t, \xi)$ by $S_f^{2,(g,\alpha)}(t, \xi)$ gives us a reconstruction by the 2nd-order SST. Since the synthesis formula for the SST and the 2nd-order SST are based on the inverse Fourier transform, it fails at the time when the IFs of two components cross.

In [21], a reconstruction algorithm based on the CT was proposed to handle this situation. We briefly summarize the ad hoc argument and the algorithm here. First, each component $f_k(x) = A_k(x)e^{2\pi i\phi_k(x)}$ is approximated locally by linear chirps: $f_k(t+x) \approx f_k(t)e^{2\pi i\phi'_k(t)x + \pi i\phi''_k(t)x^2}$, and the CT of $f_k(x)$ with window g is thus approximately

$$T_{f_k}^{(g)}(t, \xi, \lambda) \approx f_k(t)\check{g}(\xi - \phi'_k(t), \lambda - \phi''_k(t));$$

hence

$$T_f^{(g)}(t, \xi, \lambda) \approx \sum_{k=1}^K f_k(t)\check{g}(\xi - \phi'_k(t), \lambda - \phi''_k(t)).$$

Now, if $\phi'_k(t)$ and $\phi''_k(t)$ can be well approximated by some algorithms; for example, by $\omega_k(t)$ and $\mu_k(t)$ via (8) by SCT in our case, then

$$T_f^{(g)}(t, \xi, \lambda) \approx \sum_{k=1}^K \check{g}(\xi - \omega_k(t), \lambda - \mu_k(t))f_k(t).$$

By setting $(\xi, \lambda) = (\omega_l(t), \mu_l(t))$ for $l = 1, \dots, K$, we obtain a linear system:

$$\hat{\mathbf{X}}_t = \mathbf{A}_t \mathbf{X}_t,$$

where

$$\hat{\mathbf{X}}_t = \begin{bmatrix} T_f^{(g)}(t, \omega_1(t), \mu_1(t)) \\ T_f^{(g)}(t, \omega_2(t), \mu_2(t)) \\ \vdots \\ T_f^{(g)}(t, \omega_K(t), \mu_K(t)) \end{bmatrix}, \quad \mathbf{A}_t = \begin{bmatrix} a_{1,1} & a_{1,2} & \cdots & a_{1,K} \\ a_{2,1} & a_{2,2} & \cdots & a_{2,K} \\ \vdots & \vdots & \ddots & \vdots \\ a_{K,1} & a_{K,2} & \cdots & a_{K,K} \end{bmatrix}, \quad \mathbf{X}_t = \begin{bmatrix} f_1(t) \\ f_2(t) \\ \vdots \\ f_K(t) \end{bmatrix}$$

and $a_{i,j} = \check{g}(\omega_i(t) - \omega_j(t), \mu_i(t) - \mu_j(t))$, which can be obtained via an explicit expression of $\check{g}(\xi, \lambda)$ for some windows. For example, if $g(x) = e^{-\pi\alpha x^2}$, then $\check{g}(\xi, \lambda) = \frac{1}{\sqrt{\alpha+i\lambda}} e^{-\frac{\pi\xi^2}{\alpha+i\lambda}}$. The reconstruction of f_k at time t is thus achieved by

$$(9) \quad e_k^\top \mathbf{X}_t = e_k^\top \mathbf{A}_t^{-1} \hat{\mathbf{X}}_t,$$

where e_k is a unit vector with 1 in the k -th entry.

The key to the success of this algorithm is having an accurate estimate of $\phi'_k(t)$ and $\phi''_k(t)$ for the construction of \mathbf{A}_t and $\hat{\mathbf{X}}_t$; in other words, an accurate knowledge of “ridges” associated with each component in the TFC domain. As is indicated in Lemma 1, the slow decay rate of CT, and hence the low contrast of the ridges and their background, might increase the difficulty of ridge detection. To this end, we propose the following solution based on the SCT.

First, evaluate the SCT of a given signal. Second, extract ridges by the following algorithm. Suppose we know $K \geq 2$, and we want to extract $K \geq 2$ ridges by means of a fast implementation [32] of the (multiway) spectral clustering [36]. Note that K could be determined from the background knowledge. Without the background knowledge, an adaptive estimate of K from the given data is out of the scope of this paper.

- (1) Select entries in the 3-dim matrix that represent the discretization of $S_f^{(g_2)}(t, \xi, \lambda)$ whose modules are greater than q quantile of the module over all entries of the 3-dim matrix. Here we set $q = 0.9995$ or higher, and denote those entries as $\{x_i\}_{i=1}^n \subset \mathbb{R}^3$.

- (2) Form the affinity matrix W for the selected points with Gaussian kernel $g(x_i, x_j) = \exp(-\|x_i - x_j\|_2^2 / (2\sigma^2))$, and the associated degree matrix D . Here we set σ to be about the 15% percentile of all pairwise distances of $\{x_i\}_{i=1}^n$.
- (3) Compute the top $2(K-1)$ eigenvectors of the $D^{-1}W$, denoted as $u_1, \dots, u_{2(K-1)}$. Embed x_i from \mathbb{R}^3 to $(u_1(i), u_2(i), \dots, u_{2(K-1)}(i))^\top \in \mathbb{R}^{2(K-1)}$. In practice, when n is large, we suggest applying the Roseland algorithm [32].
- (4) Run k -means on the embedding to split them into K clusters (each refers to one component of the signal). For each cluster, we track back to their original samples in \mathbb{R}^3 and set those entries as the ridge of the associated component.

The ridges then represent the estimate $\phi'_k(t)$ and $\phi''_k(t)$ according to Theorem 1. We could then plug these estimates into (9). See [14] for an argument for the choice of the bandwidth σ .

3.3. Numerical implementation of SCT. The numerical implementation of SCT is by a direct discretization, which we detail now. The Matlab code is available in <https://github.com/ziyuchen7/Synchrosqueezed-chirplet-transforms>. Below we index our vectors and matrices beginning with 1. Suppose the continuous signal f is uniformly sampled over a discrete set of time points with the sampling interval $\Delta_t > 0$ second. The sampling rate is thus $f_s = \Delta_t^{-1}$. We denote the discretization of f as a column vector $\mathbf{f} \in \mathbb{R}^N$, where $\mathbf{f}(n) = f(n\Delta_t)$, where $1 \leq n \leq N$; that is, we “record” the signal for $N\Delta_t$ seconds. Choose a discrete window function $\mathbf{h} \in \mathbb{R}^{2K+1}$, where $K \in \mathbb{N}$. For example, \mathbf{h} can be a discretization of a Gaussian, so that $\mathbf{h}(K+1)$ is the center of the Gaussian. Write $\mathbf{h}', \mathbf{h}'' \in \mathbb{R}^{2K+1}$ for the discretization of the first and second derivative of the window function. Write $\mathbf{th}, \mathbf{th}', \mathbf{t}^2\mathbf{h}$ for the discretization of the entry-wise product of \mathbf{t} or \mathbf{t}^2 with \mathbf{h} or \mathbf{h}' , where $\mathbf{t}, \mathbf{t}^2 \in \mathbb{R}^{2K+1}$, $\mathbf{t}(n) = n - K - 1$ and $\mathbf{t}^2(n) = (n - K - 1)^2$, $n = 1, 2, \dots, 2K+1$. Choose a resolution $\alpha > 0$, and let $M = \lfloor \frac{0.5}{\alpha} \rfloor$, and let $M+1$ be the number of bins in the (positive) frequency axis, $2M$ be the number of bins in the chirp rate axis of our targeting TFC representation. Then, the CT of \mathbf{f} with window \mathbf{h} would be a matrix $\mathbf{T}_{\mathbf{f}}^{\mathbf{h}} \in \mathbb{C}^{2M \times (M+1) \times N}$, whose entries are

$$\mathbf{T}_{\mathbf{f}}^{\mathbf{h}}(l, m, n) = \sum_{k=1}^{2K+1} \mathbf{f}(n+k-K-1) \mathbf{h}(k) e^{\frac{-2\pi i(k-1)(m-1)}{2M}} e^{\frac{-\pi i l(k-1)^2}{4M^2}},$$

where we define $\mathbf{f}(n) = 0$ when $n < 1$ or $n > N$; $n = 1, 2, \dots, N$ is the time index; $m = 1, 2, \dots, M+1$ is the frequency index; and $l = -(M-1), \dots, M$ is the chirp rate index. The CT of \mathbf{f} with windows $\mathbf{h}', \mathbf{h}''$, $\mathbf{th}, \mathbf{th}', \mathbf{t}^2\mathbf{h}$, denoted by

$\mathbf{T}_f^{\mathbf{h}'}, \mathbf{T}_f^{\mathbf{h}''}, \mathbf{T}_f^{\mathbf{th}}, \mathbf{T}_f^{\mathbf{th}'}, \mathbf{T}_f^{\mathbf{t}^2\mathbf{h}}$ can be defined likewise. Let

$$\begin{aligned} & \lambda_f(l, m, n) \\ &= \frac{1}{2\pi}(\mathbf{T}_f^{\mathbf{h}}(l, m, n)\mathbf{T}_f^{\mathbf{h}''}(l, m, n) - 4\pi i \frac{l}{4M^2}\mathbf{T}_f^{\mathbf{h}}(l, m, n)\mathbf{T}_f^{\mathbf{th}'}(l, m, n) - 2\pi i \frac{l}{4M^2}(\mathbf{T}_f^{\mathbf{h}}(l, m, n))^2 \\ & \quad + (2\pi i \frac{l}{4M^2})^2\mathbf{T}_f^{\mathbf{h}}(l, m, n)\mathbf{T}_f^{\mathbf{t}^2\mathbf{h}}(l, m, n) - (\mathbf{T}_f^{\mathbf{h}'}(l, m, n))^2 - (2\pi i \frac{l}{4M^2})^2(\mathbf{T}_f^{\mathbf{th}}(l, m, n))^2 \\ & \quad + 4\pi i \frac{l}{4M^2}\mathbf{T}_f^{\mathbf{h}'}(l, m, n)\mathbf{T}_f^{\mathbf{th}}(l, m, n))(-\mathbf{T}_f^{\mathbf{h}}(l, m, n)\mathbf{T}_f^{\mathbf{th}'}(l, m, n) \\ & \quad + 2\pi i \frac{l}{4M^2}\mathbf{T}_f^{\mathbf{h}}(l, m, n)\mathbf{T}_f^{\mathbf{t}^2\mathbf{h}}(l, m, n) + \mathbf{T}_f^{\mathbf{th}}(l, m, n)\mathbf{T}_f^{\mathbf{h}'}(l, m, n) \\ & \quad - 2\pi i \frac{l}{4M^2}(\mathbf{T}_f^{\mathbf{th}}(l, m, n))^2)^{-1}. \end{aligned}$$

We choose a threshold $\nu > 0$ and calculate the reassignment operator:

$$\mu_f(l, m, n) = 4M^2 \text{Im}(\lambda_f(l, m, n)),$$

and

$$\omega_f(l, m, n) = m - (2M) \text{Im} \left(\frac{-\mathbf{T}_f^{\mathbf{h}'}(l, m, n)}{2\pi \mathbf{T}_f^{\mathbf{h}}(l, m, n)} - \frac{(\frac{il}{4M^2} - \lambda_f(l, m, n))\mathbf{T}_f^{\mathbf{th}}(l, m, n)}{\mathbf{T}_f^{\mathbf{h}}(l, m, n)} \right),$$

if $|\mathbf{T}_f^{\mathbf{h}}(l, m, n)| > \nu$; otherwise set $\mu_f(l, m, n) = -\infty$ and $\omega_f(l, m, n) = -\infty$. The SCT of \mathbf{f} , a matrix $\mathbf{S}_f(l, m, n) \in \mathbb{C}^{2M \times (M+1) \times N}$ is finally given by

$$\mathbf{S}_f(l, m, n) = \sum_{r, j: \mu_f(r, j, n) + M = l, \omega_f(r, j, n) = m} \mathbf{T}_f^{\mathbf{h}}(r, j, n).$$

The reconstruction of each component follows immediately.

4. NUMERICAL RESULTS

In this section, let $g_k(x) = x^k e^{-\pi x^2}$ for $k \geq 0$, unless defined otherwise. To plot the 3-dim TFC representation determined by CT or SCT, we apply the following scheme. Take q to be the 99.99% percentile of all entries of the associated discretized TFC representation. Then, plot all entries with magnitudes between different ranges by different gray scales, where we consider ranges $(l-1)q/10$ to $lq/10$, where $l = 1, \dots, 10$.

4.1. Standard linear chirps. We first look at the synthetic example shown in Figure 1, where the IFs of two ICT components cross at $t_0 = 3$ and $\xi_0 = 24$. In Figure 2, and the TF representation determined by SCT with the standard Gaussian window $g_0(x)$. Compared with the TF representation determined by other methods and CT shown in Figure 1, the TFC representation determined by SCT around the crossover time is clearer. In particular, at time $t_0 = 3$ when the IFs crossover happens at frequency $\xi_0 = 24$, the TFC representation provided by SCT is sharper compared with that provided by CT. Specifically, the magnitude at the chirp rate 0 is close to zero. This shows the impact of the squeezing step.

Next, we explore the impact of different windows. Figure 3 shows CT and SCT of f with g_0 and g_2 at different times. We observe that while both CT and SCT provide information about both components at the non-crossing time, $t_1 = 2$ s, the SCT with g_0 clearly gives a sharper representation of the frequency and chirp rate information. At the crossing time, $t_0 = 3$ s, we see a dramatic difference. On the

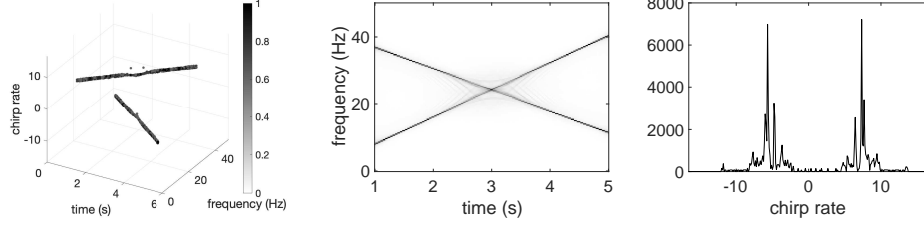


FIGURE 2. An illustration of SCT with the standard Gaussian window. From left to right: the 3-dim visualization of $|S_f^{(g_0)}(t, \xi, \lambda)|$, the projection of $|S_f^{(g_0)}(t, \xi, \lambda)|$ onto the time-frequency plane, and the plot of $|S_f^{(g_0)}(t_0, \xi_0, \lambda)|$, where $t_0 = 3$ and $\xi_0 = 24$. For each time-frequency representation, we set all entries with the magnitude above the 99.99% percentile of all entries to be the magnitude of the 99.99% percentile.

one hand, we cannot easily distinguish the chirp rates of the two components at the crossing frequency 24 Hz when CT is applied. On the other hand, we can get the wanted information when SCT with g_0 is applied, and a sharper representation of the chirp rate information when g_2 is used as the window. We further show the results with g_2 as the window in Figure 4. Compared with CT with g_0 shown in Figure 1, we see that CT with g_2 gives a sharper TFC representation and hence the TF representation, which reflects the theoretical results shown in Proposition 5. On the other hand, SCT gives us a more concentrated representation of the chirp rate information compared with CT. Moreover, we see that the chirp rate locations of the peaks by SCT with g_0 are at -5.67 and 7.33 , and the peak locations in the SCT with window g_2 are at -6.33 and 8 , and we know that the true chirp rates of f_1 and f_2 are -2π (≈ -6.28) and 8 . Clearly, the SCT with g_2 gives a better estimate of IF and chirp rate. Moreover, two ridges extracted from $|S_f^{(g_2)}(t, \xi, \lambda)|$ by our proposed algorithm in Section 3.2 is shown in Figure 4. Furthermore, we compare SCT with different windows, including $g_3(x) = x^2 e^{-5\pi x^2}$, $g_4(x) = x^4 e^{-5\pi x^2}$ and $g_5(x) = x^6 e^{-5\pi x^2}$ at the frequency-crossover time. The results are shown in Figure 5. It shows that g_4 seems to give the most concentrated TFC representation in the chirp rate direction in both CT and SCT. Note that while this finding seems to be against Proposition 6, which states that the window obtained by multiplying the Gaussian $e^{-\pi x^2}$ with higher power x^n gives us a better TFC representation of SCT in the chirp rate direction, we mention that the analysis is asymptotic, and it is not necessarily guaranteed that increasing n to a finite number with α fixed (as g_4 and g_5 here) will give us better concentration, particularly under the numerical precision. This result suggests the value of an extensive exploration of the window effect on CT and SCT. However, it is out of the scope of this paper, and more detailed analysis will be reported in our future work.

Third, we evaluate how the squeezing step functions; that is, how does the squeezing step rearrange the TFC representation determined by CT. Consider the following way to *invert SCT*. Choose $\epsilon_1, \epsilon_2 > 0$, and define the inverse SCT of f

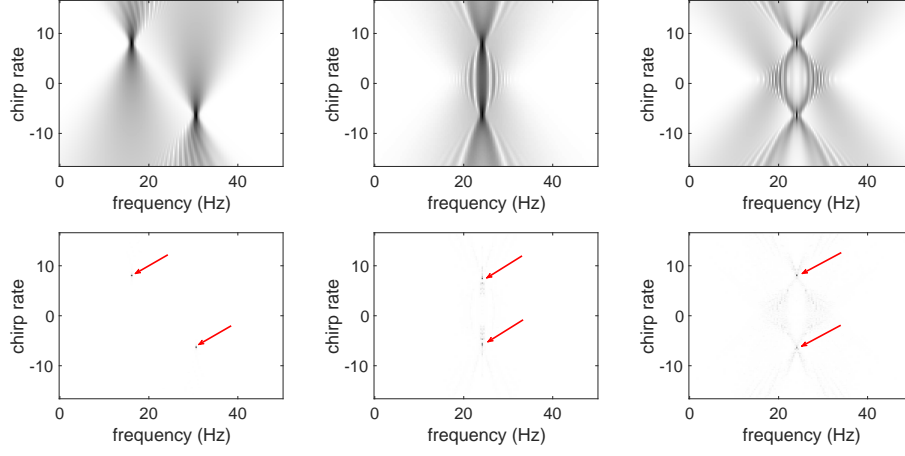


FIGURE 3. An illustration of the impact of windows. Consider $g_0(x) = e^{-\pi x^2}$ and $g_2(x) = x^2 e^{-\pi x^2}$. Top row, from left to right: $|T_f^{(g_0)}(t_1, \xi, \lambda)|$, $|T_f^{(g_0)}(t_0, \xi, \lambda)|$, and $|T_f^{(g_2)}(t_0, \xi, \lambda)|$. Bottom row, from left to right: $|S_f^{(g_0)}(t_1, \xi, \lambda)|$, $|S_f^{(g_0)}(t_0, \xi, \lambda)|$, and $|S_f^{(g_2)}(t_0, \xi, \lambda)|$. To enhance the visualization, the red arrows are superimposed to indicate the squeezed “spots”.

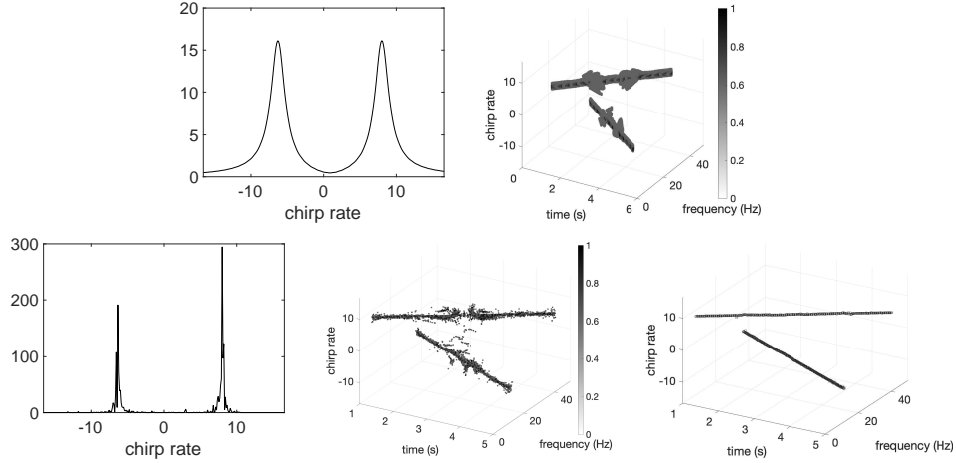


FIGURE 4. Top row, from left to right: $|T_f^{(g_2)}(t_0, \xi_0, \lambda)|$, and the 3-dim visualization of $|T_f^{(g_2)}(t, \xi, \lambda)|$. Bottom row, from left to right: $|S_f^{(g_0)}(t_0, \xi_0, \lambda)|$, the 3-dim visualization of $|S_f^{(g_2)}(t, \xi, \lambda)|$, and the ridges extracted from $|S_f^{(g_2)}(t, \xi, \lambda)|$.

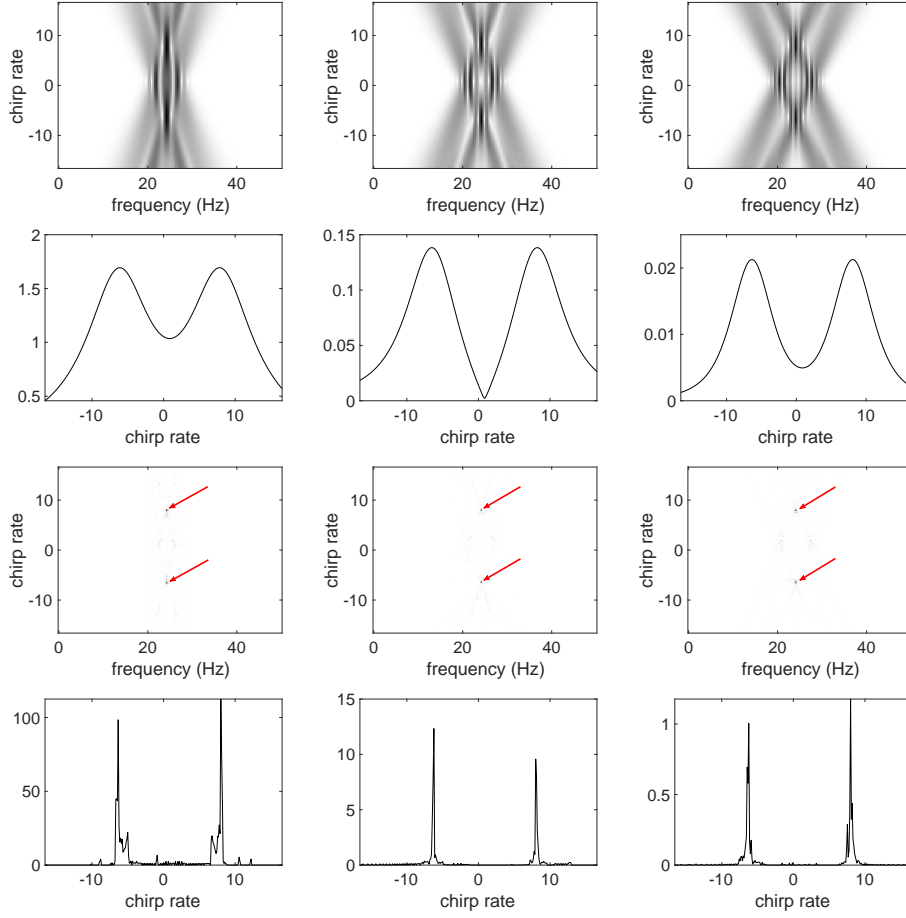


FIGURE 5. Top left: plot of $|T_f^{(g_3)}(t_0, \xi, \lambda)|$; top middle: plot of $|T_f^{(g_4)}(t_0, \xi, \lambda)|$; top right: plot of $|T_f^{(g_5)}(t_0, \xi, \lambda)|$; second row left: plot of $|T_f^{(g_3)}(t_0, \xi_0, \lambda)|$; second row middle: plot of $|T_f^{(g_4)}(t_0, \xi_0, \lambda)|$; second row right: plot of $|T_f^{(g_5)}(t_0, \xi_0, \lambda)|$; third row left: plot of $|S_f^{(g_3)}(t_0, \xi, \lambda)|$; third row middle: plot of $|S_f^{(g_4)}(t_0, \xi, \lambda)|$; third row right: plot of $|S_f^{(g_5)}(t_0, \xi, \lambda)|$; bottom left: plot of $|S_f^{(g_3)}(t_0, \xi_0, \lambda)|$; bottom middle: plot of $|S_f^{(g_4)}(t_0, \xi_0, \lambda)|$; bottom right: plot of $|S_f^{(g_5)}(t_0, \xi_0, \lambda)|$.

with window g in the vicinity of (t, ξ, λ) as a set:

$$Q_{\epsilon_1, \epsilon_2}(t, \xi, \lambda) = \{(t, \eta, \gamma) \mid |\omega_f^{(g)}(t, \eta, \gamma) - \xi| < \epsilon_1 \text{ and } |\mu_f^{(g)}(t, \eta, \gamma) - \lambda| < \epsilon_2\}.$$

Figure 6 shows the inverted SCT of $f(x)$ in the vicinity of the ridge of f_1 (extracted from $S_f^{(g_2)}$) with g_0 and g_2 at t_0 and t_1 . Here we choose $\epsilon_1 = 1, \epsilon_2 = 0.33$. It is clear that there is an interesting “pattern” in the nonlinear squeezing step in SCT, which comes from the nonlinearity of the squeezing step.

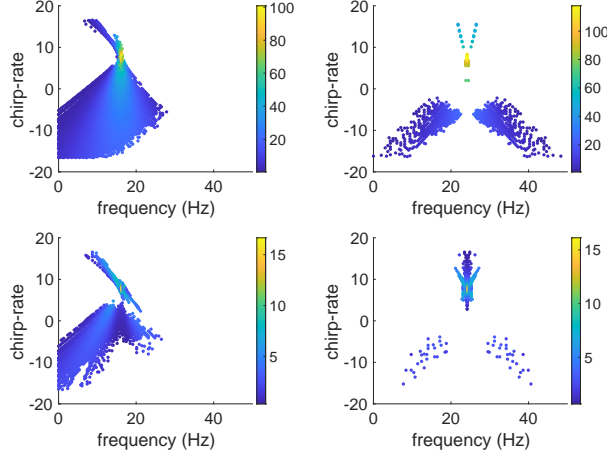


FIGURE 6. Top left: inverse SCT map of the vicinity of the ridge of f_1 with g_0 at $t_1 = 2$ s; top right: inverse SCT map of the vicinity of the ridge of f_1 with g_0 at $t_0 = 3$ s; bottom left: inverse SCT map of the vicinity of the ridge of f_1 with g_2 at $t_1 = 2$ s; bottom right: inverse SCT map of the vicinity of the ridge of f_1 with g_2 at $t_0 = 3$ s. Color reflects the magnitude of the CT.

Finally, we evaluate the proposed reconstruction approach. Figure 7 shows the reconstructed f_1 and f_2 by the proposed reconstruction scheme with window g_0 [21], denoted by f_1^G, f_2^G , where the IF and chirp rate information is obtained by the SCT of f with window g_2 . For a comparison purpose, the reconstructions of f_1 and f_2 through the reconstruction of 2nd-order SST around ridges of f_1 and f_2 , denoted by f_1^S, f_2^S , are also provided. We see that the reconstruction is good except near t_0 of the crossover frequency. Quantitatively, we evaluate the reconstruction errors over two disjoint intervals, $\mathcal{I}_1 = [2.5, 3.5]$ (around the crossover time) and $\mathcal{I}_2 = [1, 2.5) \cup (3.5, 5]$ (away from the crossover time), where we have $\frac{\|(\Re(f_1^G) - \Re(f_1))\mathbf{1}_{\mathcal{I}_1}\|_2}{\|\Re(f_1)\mathbf{1}_{\mathcal{I}_1}\|_2} = 0.076$, $\frac{\|(\Re(f_1^G) - \Re(f_1))\mathbf{1}_{\mathcal{I}_2}\|_2}{\|\Re(f_1)\mathbf{1}_{\mathcal{I}_2}\|_2} = 0.064$, $\frac{\|(\Re(f_1^S) - \Re(f_1))\mathbf{1}_{\mathcal{I}_1}\|_2}{\|\Re(f_1)\mathbf{1}_{\mathcal{I}_1}\|_2} = 0.458$, and $\frac{\|(\Re(f_1^S) - \Re(f_1))\mathbf{1}_{\mathcal{I}_2}\|_2}{\|\Re(f_1)\mathbf{1}_{\mathcal{I}_2}\|_2} = 0.021$. We see from this example that the reconstruction error by SCT is reduced at the crossing time t_0 , but it is worse at the non-crossing time if we compare it with the reconstruction by the 2nd-order SST.

4.2. Simulated time-varying chirp rate signal. Next, we demonstrate the performance of SCT on signals with time-varying amplitudes, frequencies and chirp rates. We use the smoothed Brownian path realizations to model the AM, IF and the time-varying chirp rates of the constituent components of the signal. This simulation scheme is a generalization of that proposed in [13] and we summarize it here. If W is the standard Brownian motion defined on $[0, \infty)$, then we define the

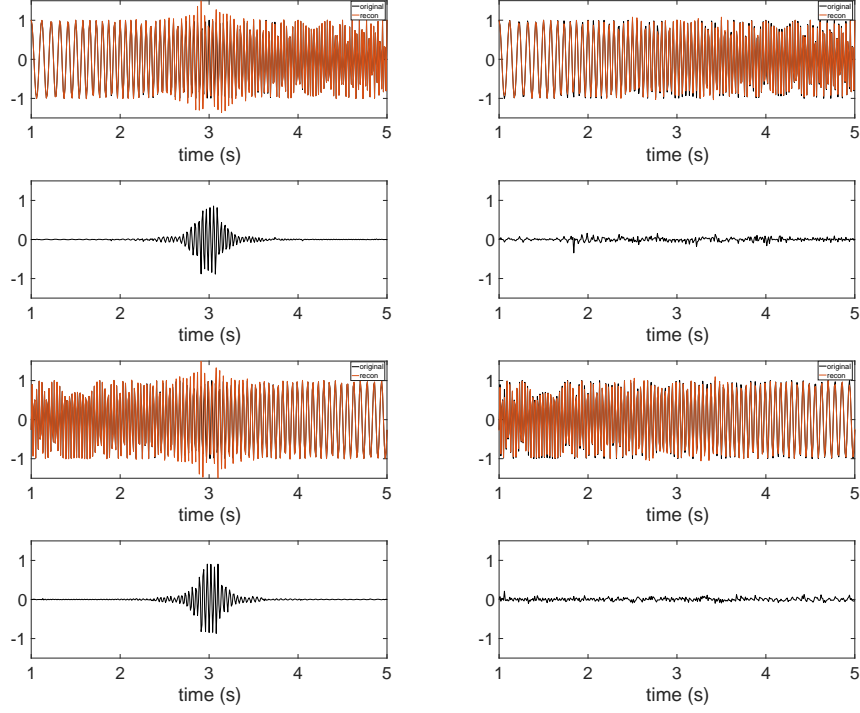


FIGURE 7. Left column: reconstruction of signals from STFT-based 2nd-order SST with window g_0 . Top row: reconstruction of $\Re(f_1)$; second row: reconstruction error of $\Re(f_1)$; third row: reconstruction of $\Re(f_2)$; bottom row: reconstruction error of $\Re(f_2)$. Right column: reconstruction of signals using group idea with window g_0 with instantaneous frequencies and chirp rates obtained on ridges extracted from $|S_f^{(g_2)}(t, \xi, \lambda)|$ (as shown in Figure 4 bottom). Top row: reconstruction of $\Re(f_1)$; second row: reconstruction error of $\Re(f_1)$; third row: reconstruction of $\Re(f_2)$; bottom row: reconstruction error of $\Re(f_2)$.

smoothed Brownian motion with bandwidth $B > 0$ as $\Phi_B := W \star K_B$, where K_B is the Gaussian function with standard deviation $B > 0$ and \star denotes the convolution operator. Given $T > 0$ and parameters $\zeta_1, \dots, \zeta_6 > 0$, we then define the following family of random processes on $[0, T]$:

$$\Psi_{[\zeta_1, \dots, \zeta_7]}(x) := \zeta_1 + \zeta_2 x + \zeta_3 x^2 + \zeta_4 \frac{\Phi_{\zeta_5}(x)}{\|\Phi_{\zeta_5}\|_{L^\infty[0, T]}} + \zeta_6 \int_0^x \int_0^u \frac{\Phi_{\zeta_7}(s)}{\|\Phi_{\zeta_7}\|_{L^\infty[0, T]}} ds du.$$

For the amplitude $A(x)$ of each component, we set $\zeta_2 = \zeta_3 = \zeta_6 = 0$; every realization then varies smoothly between ζ_1 and $\zeta_1 + \zeta_4$. In the example shown below, the signal consists of two components (i.e. $K = 2$) on $[0, 10]$; their two amplitudes are independent realizations of $\Psi_{[2, 0, 0, 1, 200, 0, 0]}(x)$. To simulate phase functions, we set $\zeta_1 = \zeta_4 = 0$. In this example we consider, we take for $\phi_1(x)$ a realization of $\Psi_{[0, 1, 4.5, 0, 0, 0, 2, 400]}(x)$, and for $\phi_2(t)$ a realization of $\Psi_{[0, 12, -4, 0, 0, 0, 25, 300]}(x)$. The

signal is then

$$s(x) := f_1(x) + f_2(x) = A_1(x)e^{2\pi i\phi_1(x)} + A_2(x)e^{2\pi i\phi_2(x)},$$

where $x \in [0, 10]$, and the sampling rate is 100Hz. Finally, we add white noise $\eta(x)$ to $s(x)$, where the noise are identically distributed Student t_4 random variables, so the resulting signal is $f(x) = s(x) + \eta(x)$. To avoid the boundary effects of our TF method, we only show the result for $x \in [1, 9]$.

Figure 8 gives the plot of the signals and their IFs and chirp rates. The signal-to-noise ratio is 5.20, computed as $20 \log_{10}(\frac{\text{std}(f(x))}{\text{std}(\xi(x))})$, where std stands for standard deviation. Also, a comparison of TF representations determined by the 2nd-order SST and the SCT with different window functions $g_0(x)$ and $g_2(x)$ is shown. We see that with SCT, the TF representation gives sharper information around the time when IF crossover happens. Figure 9 shows a comparison of CT and SCT with different window functions $g_0(x)$ and $g_2(x)$ at the IF crossover time. We see that SCT with g_2 gives two peaks that are exactly located at the true instantaneous chirp rates of f_1 and f_2 . Figure 10 shows the reconstruction of f_1 and f_2 from the proposed reconstruction scheme with window g_0 , where we consider both the situations that we know the true IFs and instantaneous chirp rates or when the IFs and instantaneous chirp rates are estimated from $S_f^{(g_2)}(t, \xi, \lambda)$. We see that the estimated IFs and instantaneous chirp rate from SCT give almost identical results.

Finally, we provide a quantitative result. Define the relative reconstruction error between the estimated signal \tilde{f} and the original clean signal f as $\frac{\|\tilde{f}-f\|_2}{\|f\|_2}$. We report the mean and standard deviation (SD) of the relative reconstruction error of $\Re(f_1)$ and $\Re(f_2)$ over 100 different realizations of the signal and noise, where their IFs and instantaneous chirp rates are extracted from SCT, $S_f^{(g_2)}(t, \xi, \lambda)$. The mean \pm SD of $\frac{\|\Re(\tilde{f}_1)-\Re(f_1)\|_2}{\|\Re(f_1)\|_2}$ and $\frac{\|\Re(\tilde{f}_2)-\Re(f_2)\|_2}{\|\Re(f_2)\|_2}$ are 0.154 ± 0.091 and 0.161 ± 0.084 respectively. We also report the mean and SD of the optimal transport (OT) distance between the estimated $\tilde{\phi}'_k$ from $S_f^{(g_2)}(t, \xi, \lambda)$ and ϕ'_k , as well as $\hat{\phi}'_k$ from $T_f^{(g_2)}(t, \xi, \lambda)$ and ϕ'_k , where $k = 1, 2$. The OT distance is obtained by first computing the 1-dimensional Wasserstein-1 distance between $\tilde{\phi}'_k(x)$ (or $\hat{\phi}'_k(x)$) and $\phi'_k(x)$, where $k = 1, 2$, at every time x using the Euclidean distance as metric, and then taking average over all $x \in [1, 9]$. The resulting mean \pm SD for $\text{OT}(\tilde{\phi}'_1, \phi'_1)$, $\text{OT}(\hat{\phi}'_1, \phi'_1)$, $\text{OT}(\tilde{\phi}'_2, \phi'_2)$ and $\text{OT}(\hat{\phi}'_2, \phi'_2)$ are 0.424 ± 0.280 , 0.854 ± 1.778 , 0.325 ± 0.252 , and 0.453 ± 0.728 respectively. We conclude that the IFs estimated from $S_f^{(g_2)}(t, \xi, \lambda)$ are more accurate than those estimated from $T_f^{(g_2)}(t, \xi, \lambda)$.

4.3. Wolf Howling Signal. We now show a real world data analysis. An important issue in conservation biology is to estimate the number of wolves in the field [30, 16]. In this final example we show the numerical result with a wolf howling signal. The sound is downloaded from Wolf Park website.¹ The signal f is sampled at 8 kHz for 55 s. In this example, we downsample the signal f by a factor 8 to look at the crossover IFs, which is below 500Hz. Figure 11 shows the signal and the TFC representation and the associated TF representation determined by CT and SCT with g_0 . Figure 12 shows the frequency-chirp rate slices at three instants 16.16s, 16.43s and 16.57s with window g_0 and g_2 . We see in Figure 12 that at

¹<https://wolfpark.org/Images/Resources/Howls/>

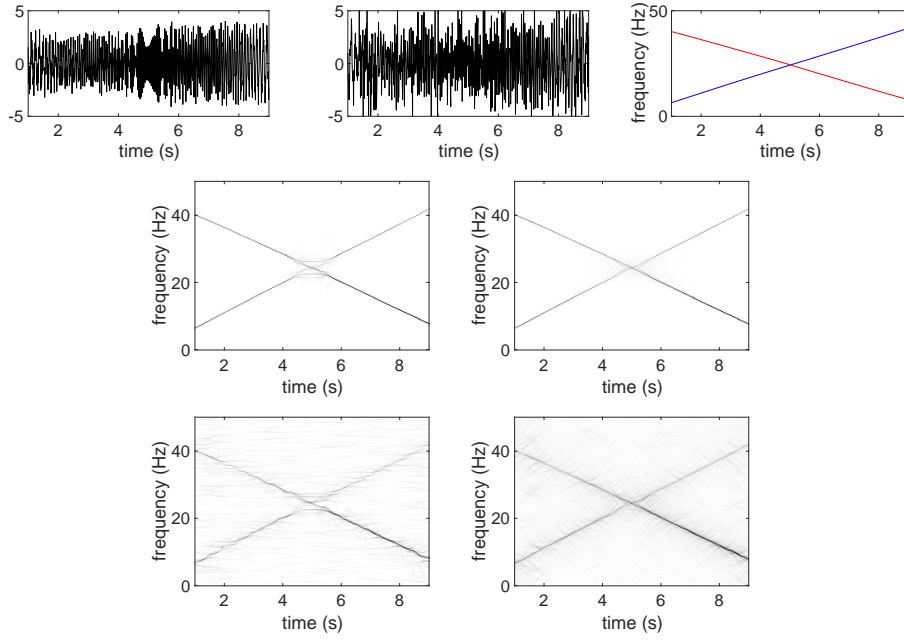


FIGURE 8. Top left, from left to right: the clean signal $\Re(s)$, the noisy signal $\Re(f)$, and the plot of ϕ'_1 and ϕ'_2 . Note that the IFs have a crossing point at $(t_0, \xi_0) = (4.66, 7.8)$. Second row, from left to right: 2nd-order SST of the clean signal s with g_0 and the TF representation determined by projecting the SCT with g_0 . Bottom row, from left to right: 2nd-order SST of the noisy signal f with g_0 and the TF representation determined by projecting the SCT with g_0 .

16.16s, the IFs of the two components (two wolves) are well-separated. We do not expect any problem and the SCT with g_0 gives a clear representation of their IFs and ICs, particularly in the chirp rate axis compared with CT. At about 16.43s, when their IFs are very close and their ICs are reasonably separated, two components are mixed in the chirp rate direction in the SCT with g_0 ; however, we can observe two places of concentration in the frequency-chirp rate slice of the SCT with g_2 , which is also sharper compared to the CT at that time. At 16.57s near another instance of frequency crossover, their chirp rates are close, and it becomes hard to distinguish those two components even in the SCT with g_2 . While solving this wolf counting problem is out of the scope of this paper, we leave this problem to the future work.

5. DISCUSSION AND FUTURE WORK

While the proposed SCT algorithm could help disentangle components with crossover IFs, there are still several open problems. First, we need a fast implementation of the SCT algorithm for large databases, probably by including the existing fast implementation for CT [23]. Unlike SST and its variations, at each time, the computational time depends on the frequency axis only, in SCT, at each

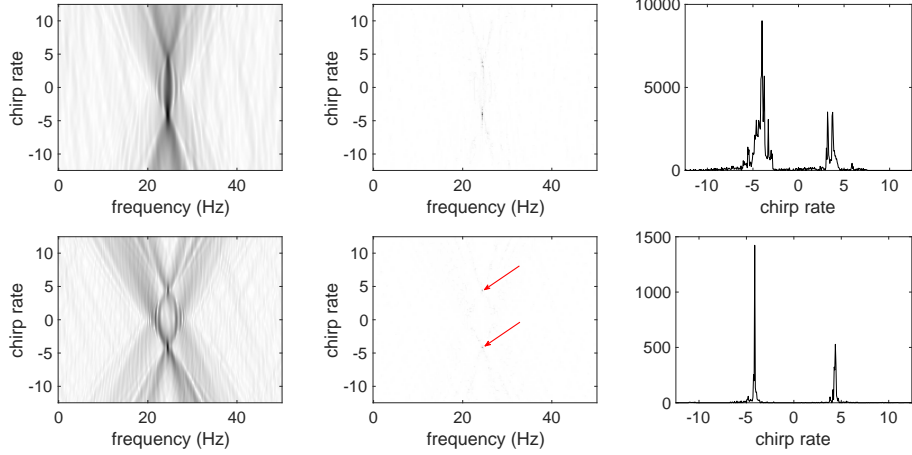


FIGURE 9. Top left: plot of $|T_f^{(g_0)}(t_0, \xi, \lambda)|$; top middle: plot of $|S_f^{(g_0)}(t_0, \xi, \lambda)|$; top right: plot of $|S_f^{(g_0)}(t_0, \xi_0, \lambda)|$; bottom left: plot of $|T_f^{(g_2)}(t_0, \xi, \lambda)|$; bottom middle: plot of $|T_f^{(g_2)}(t_0, \xi, \lambda)|$ with arrows pointing out concentrations; bottom right: plot of $|S_f^{(g_2)}(t_0, \xi_0, \lambda)|$.

time, the computational time depends on both the frequency axis and chirp rate axis. An intuitive solution is taking a reliable TF representation to determine those frequency entries are “informative”, and focus on those frequency entries to evaluate information on the chirp rate. However, this solution might be challenged by the nonlinear relationship between frequency and chirp rate shown in Figure 6. We will systematically study how to design a fast implementation of SCT (or even CT) in our future work.

The oscillatory components, or modes, considered in this paper are all sinusoidal; that is, it is the cosine function as an 1-periodic signal that is stretched (by the phase function) and/or scaled (by the AM). In practice, we found many signals oscillate with a non-sinusoidal pattern (or wave-shape function) [38]. It would be an interesting topic to extend SCT to the signals with non-sinusoidal wave-shape functions. For example, while the cepstrum is used to handle the impact of non-sinusoidal wave-shape function on the spectrogram, what is the proper geometric, or algebraic structure, on the TFC plane that we can count to handle the non-sinusoidal wave-shape functions?

The ϵ -ICT function is nothing but a generalization of the linear chirp function, where locally it behaves like a linear chirp function; that is, locally, the phase function of an ϵ -ICT function is close to a quadratic function. A natural question to ask is what if the phase function is a polynomial? Such a problem has been considered in [2, 35], among many others. Since our theory for SCT is based on the ϵ -ICT assumption, we cannot guarantee what may happen when we apply SCT to a signal with polynomial phase. However, based on our experience in applying SST to estimate IF when the chirp rate is non-trivial (the estimate is

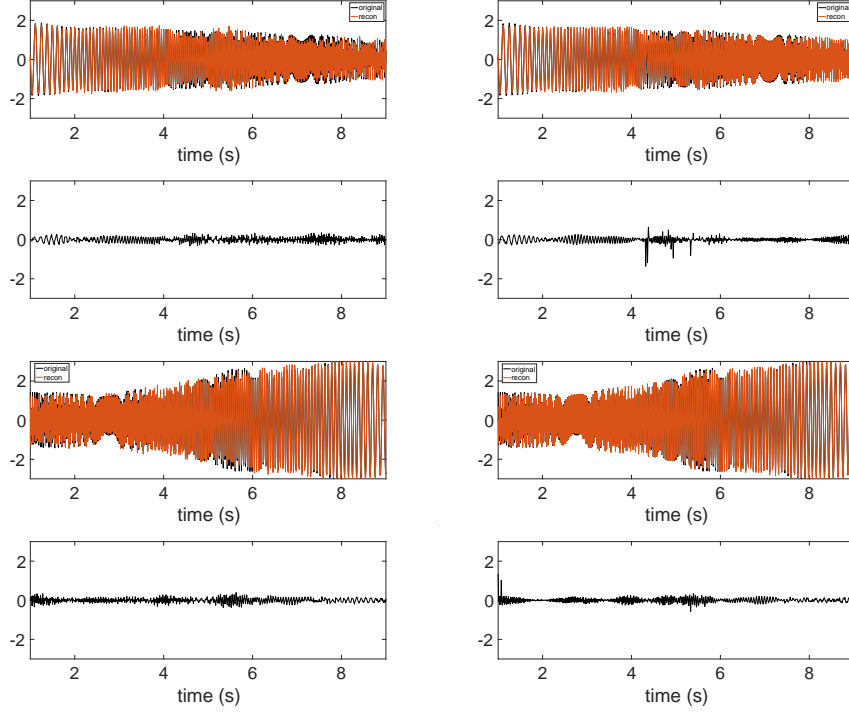


FIGURE 10. Left column: reconstruction of signals using group idea with window g_0 , assuming we know the true instantaneous frequency and chirp rate. Top row: reconstruction of $\Re(f_1)$; second row: reconstruction error of $\Re(f_1)$; third row: reconstruction of $\Re(f_2)$; bottom row: reconstruction error of $\Re(f_2)$. Right column: reconstruction of signals using group idea with window g_0 , the instantaneous frequency and chirp rate are extracted from $S_f^{(g_2)}$. Top row: reconstruction of $\Re(f_1)$; second row: reconstruction error of $\Re(f_1)$; third row: reconstruction of $\Re(f_2)$; bottom row: reconstruction error of $\Re(f_2)$.

biased, and the bias depends on the chirp rate, which leads to the 2nd-order SST and other variations), we would expect biased IF and chirp rate estimates under some relationships between IF and chirp rates.

Last but not the least, while we empirically see that SCT is robust to noise (e.g. Figure 8), we do not have a theoretical justification at this moment. Note that while we use differentiation to motivate the squeezing step of SCT, that squeezing step can be evaluated by different windows without any differentiation. We could thus apply the same argument as that in [10]. Moreover, we may generalize the technique used in [33] to obtain the impact of noise on the TFC representation, or the distribution of the TF representation under the non-null setup. We will leave the above interesting problems in our future work.

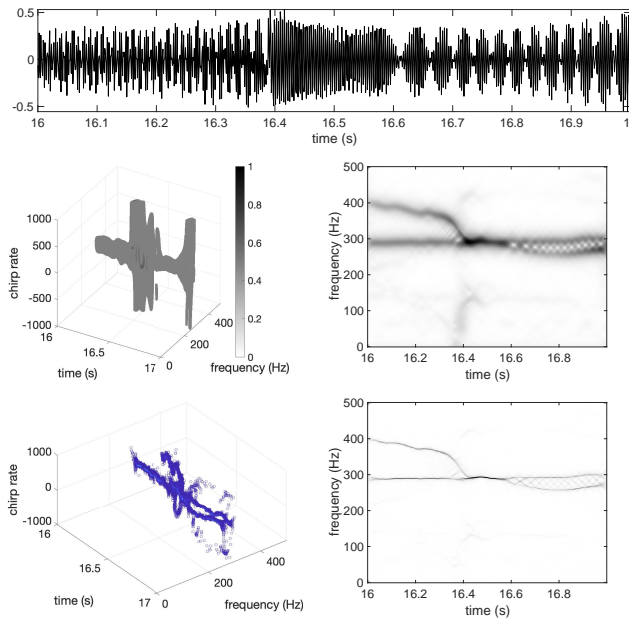


FIGURE 11. Top: a wolf howling signal between 16 and 17 seconds. Second row: the chirplet transform of the signal with a Gaussian window with the half window width 0.16 second and its associated TF representation. Third row: the synchrosqueezed chirplet transform of the signal with the same window and its associated TF representation.

REFERENCES

- [1] F. AUGER AND P. FLANDRIN, *Improving the readability of time-frequency and time-scale representations by the reassignment method*, IEEE Transactions on signal processing, 43 (1995), pp. 1068–1089.
- [2] B. BARKAT AND B. BOASHASH, *Instantaneous frequency estimation of polynomial fm signals using the peak of the pwvd: Statistical performance in the presence of additive gaussian noise*, IEEE Transactions on Signal Processing, 47 (1999), pp. 2480–2490.
- [3] R. BEHERA, S. MEIGNEN, AND T. OBERLIN, *Theoretical analysis of the second-order synchrosqueezing transform*, Applied and Computational Harmonic Analysis, 45 (2018), pp. 379–404.
- [4] B. BOASHASH AND P. O’SHEA, *Polynomial wigner-ville distributions and their relationship to time-varying higher order spectra*, IEEE Transactions on Signal Processing, 42 (1994), pp. 216–220.
- [5] B. BOASHASH AND B. RISTIC, *Polynomial time-frequency distributions and time-varying higher order spectra: application to the analysis of multicomponent fm signals and to the treatment of multiplicative noise*, Signal Processing, 67 (1998), pp. 1–23.
- [6] F. BOSSMANN AND J. MA, *Asymmetric chirplet transform for sparse representation of seismic data*, Geophysics, 80 (2015), pp. WD89–WD100.
- [7] E. J. CANDLES, *Multiscale chirplets and near-optimal recovery of chirps*, Tech. Rep., Technical Report, Stanford University, (2002).
- [8] E. J. CANDLES, P. R. CHARLTON, AND H. HELGASON, *Detecting highly oscillatory signals by chirplet path pursuit*, Applied and Computational Harmonic Analysis, 24 (2008), pp. 14–40.
- [9] R. A. CARMONA, W. L. HWANG, AND B. TORRÉSANI, *Characterization of signals by the ridges of their wavelet transforms*, IEEE transactions on signal processing, 45 (1997), pp. 2586–2590.

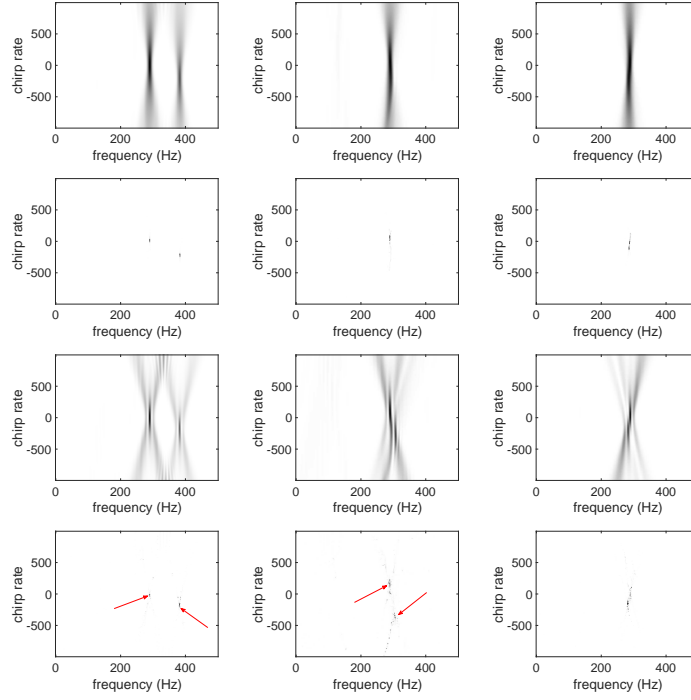


FIGURE 12. Top row, from left to right: $\left|T_f^{(g_0)}(16.16, \xi, \lambda)\right|^2$, $\left|T_f^{(g_0)}(16.43, \xi, \lambda)\right|^2$, and $\left|T_f^{(g_0)}(16.57, \xi, \lambda)\right|^2$. Second row, from left to right: $\left|S_f^{(g_0)}(16.16, \xi, \lambda)\right|^2$, $\left|S_f^{(g_0)}(16.43, \xi, \lambda)\right|^2$ and $\left|S_f^{(g_0)}(16.57, \xi, \lambda)\right|^2$. Third row, from left to right: $\left|T_f^{(g_2)}(16.16, \xi, \lambda)\right|^2$, $\left|T_f^{(g_2)}(16.43, \xi, \lambda)\right|^2$, and $\left|T_f^{(g_2)}(16.57, \xi, \lambda)\right|^2$. Bottom row, from left to right: $\left|S_f^{(g_2)}(16.16, \xi, \lambda)\right|^2$, $\left|S_f^{(g_2)}(16.43, \xi, \lambda)\right|^2$ and $\left|S_f^{(g_2)}(16.57, \xi, \lambda)\right|^2$. Red arrows are imposed to enhance the visualization.

- [10] Y.-C. CHEN, M.-Y. CHENG, AND H.-T. WU, *Non-parametric and adaptive modelling of dynamic periodicity and trend with heteroscedastic and dependent errors*, J. R. Stat. Soc. Ser. B. Stat. Methodol., 76 (2014), pp. 651–682.
- [11] J. CUI, W. WONG, AND S. MANN, *Time-frequency analysis of visual evoked potentials using chirplet transform*, Electronics Letters, 41 (2005), pp. 217–218.
- [12] I. DAUBECHIES, J. LU, AND H.-T. WU, *Synchrosqueezed wavelet transforms: An empirical mode decomposition-like tool*, Applied and computational harmonic analysis, 30 (2011), pp. 243–261.
- [13] I. DAUBECHIES, Y. WANG, AND H.-T. WU, *ConceFT: Concentration of frequency and time via a multitapered synchrosqueezed transform*, Philos. Trans. R. Soc. A-Math. Phys. Eng. Sci., 374 (2016), p. 20150193.
- [14] X. DING AND H.-T. WU, *Impact of signal-to-noise ratio and bandwidth on graph laplacian spectrum from high-dimensional noisy point cloud*, 2021.

- [15] I. DJUROVIĆ, *Qml-ransac instantaneous frequency estimator for overlapping multicomponent signals in the time-frequency plane*, IEEE Signal Processing Letters, 25 (2018), pp. 447–451.
- [16] B. DUGNOL, C. FERNÁNDEZ, G. GALIANO, AND J. VELASCO, *On a chirplet transform-based method applied to separating and counting wolf howls*, Signal Processing, 88 (2008), pp. 1817–1826.
- [17] P. FLANDRIN, *Time-frequency/time-scale analysis*, vol. 10 of Wavelet Analysis and its Applications, Academic Press Inc., San Diego, 1999.
- [18] S. K. GHOSH, R. PONNALAGU, R. TRIPATHY, AND U. R. ACHARYA, *Automated detection of heart valve diseases using chirplet transform and multiclass composite classifier with pcg signals*, Computers in biology and medicine, 118 (2020), p. 103632.
- [19] D. HARTONO, D. HALIM, AND G. W. ROBERTS, *Gear fault diagnosis using the general linear chirplet transform with vibration and acoustic measurements*, Journal of Low Frequency Noise, Vibration and Active Control, 38 (2019), pp. 36–52.
- [20] N. E. HUANG, Z. SHEN, S. R. LONG, M. C. WU, H. H. SHIH, Q. ZHENG, N.-C. YEN, C. C. TUNG, AND H. H. LIU, *The empirical mode decomposition and the hilbert spectrum for non-linear and non-stationary time series analysis*, Proceedings of the Royal Society of London. Series A: mathematical, physical and engineering sciences, 454 (1998), pp. 903–995.
- [21] L. LI, N. HAN, Q. JIANG, AND C. K. CHUI, *A chirplet transform-based mode retrieval method for multicomponent signals with crossover instantaneous frequencies*, Digital Signal Processing, (2021), p. 103262.
- [22] P. LI AND Q.-H. ZHANG, *If estimation of overlapped multicomponent signals based on viterbi algorithm*, Circuits, Systems, and Signal Processing, 39 (2020), pp. 3105–3124.
- [23] Y. LU, E. ORUKLU, AND J. SANIIE, *Fast chirplet transform with fpga-based implementation*, IEEE Signal Processing Letters, 15 (2008), pp. 577–580.
- [24] S. MANN AND S. HAYKIN, *Time-frequency perspectives: The chirplet transform*, IEEE ICASSP-92, San Francisco, (1992).
- [25] S. MANN AND S. HAYKIN, *‘chirplets’ and ‘warblers’: Novel time–frequency methods*, Electronics letters, 28 (1992), pp. 114–116.
- [26] ———, *The chirplet transform: Physical considerations*, IEEE Transactions on Signal Processing, 43 (1995), pp. 2745–2761.
- [27] M. NAHON, *Phase Evaluation and Segmentation*, PhD thesis, Yale University, New Haven, 2000.
- [28] T. OBERLIN AND S. MEIGNEN, *The second-order wavelet synchrosqueezing transform*, in 2017 IEEE International Conference on Acoustics, Speech and Signal Processing (ICASSP), IEEE, 2017, pp. 3994–3998.
- [29] T. OBERLIN, S. MEIGNEN, AND V. PERRIER, *Second-order synchrosqueezing transform or invertible reassignment? towards ideal time-frequency representations*, IEEE transactions on signal processing, 63 (2015), pp. 1335–1344.
- [30] D. PASSILONGO, L. MATTIOLI, E. BASSI, L. SZABÓ, AND M. APOLLONIO, *Visualizing sound: counting wolves by using a spectral view of the chorus howling*, Frontiers in zoology, 12 (2015), pp. 1–10.
- [31] D. B. PERCIVAL AND A. T. WALDEN, *Spectral Analysis for Physical Applications: Multitaper and Conventional Univariate Techniques*, Cambridge University Press, 1993.
- [32] C. SHEN AND H.-T. WU, *Scalability and robustness of spectral embedding: landmark diffusion is all you need*, arXiv preprint arXiv:2001.00801, (2020).
- [33] M. SOURISSEAU, H.-T. WU, AND Z. ZHOU, *Inference of synchrosqueezing transform–toward a unified statistical analysis of nonlinear-type time-frequency analysis*, arXiv preprint arXiv:1904.09534, (2019).
- [34] G. THAKUR AND H.-T. WU, *Synchrosqueezing-based recovery of instantaneous frequency from nonuniform samples*, SIAM Journal on Mathematical Analysis, 43 (2011), pp. 2078–2095.
- [35] X. TU, Y. HU, F. LI, S. ABBAS, AND Y. LIU, *Instantaneous frequency estimation for nonlinear fm signal based on modified polynomial chirplet transform*, IEEE Transactions on Instrumentation and Measurement, 66 (2017), pp. 2898–2908.
- [36] U. VON LUXBURG, *A tutorial on spectral clustering*, Statistics and computing, 17 (2007), pp. 395–416.
- [37] G. WANG, X.-G. XIA, B. T. ROOT, V. C. CHEN, Y. ZHANG, AND M. AMIN, *Manoeuvring target detection in over-the-horizon radar using adaptive clutter rejection and adaptive chirplet transform*, IEE Proceedings-Radar, Sonar and Navigation, 150 (2003), pp. 292–298.

- [38] H.-T. WU, *Instantaneous frequency and wave shape functions (I)*, Appl. Comput. Harmon. Anal., 35 (2013), pp. 181–199.
- [39] H.-T. WU, *Current state of nonlinear-type time-frequency analysis and applications to high-frequency biomedical signals*, Current Opinion in Systems Biology, (2020).
- [40] X.-G. XIA, *Discrete chirp-fourier transform and its application to chirp rate estimation*, IEEE Transactions on Signal processing, 48 (2000), pp. 3122–3133.
- [41] X. ZHU, H. YANG, Z. ZHANG, J. GAO, AND N. LIU, *Frequency-chirprate reassignment*, Digital Signal Processing, 104 (2020), p. 102783.
- [42] X. ZHU, Z. ZHANG, Z. LI, J. GAO, X. HUANG, AND G. WEN, *Multiple squeezes from adaptive chirplet transform*, Signal Processing, 163 (2019), pp. 26–40.

APPENDIX A. PROOF OF THEOREM 1

In this supplementary section, we list the lemmas that make up the proof of Theorem 1.

Lemma 3. For any tuple (t, ξ, λ) under consideration, there can be at most one $k \in \{1, \dots, K\}$ such that $|\xi - \phi'_k(t)| + |\lambda - \phi''_k(t)| < \Delta$, i.e. $(t, \xi, \lambda) \in Z_k$.

Proof. Assume there exists $(t, \xi, \lambda) \in Z_k \cap Z_l$ for $k \neq l$, then by the definition of Z_k we have

$$\begin{aligned} |\phi'_k(t) - \phi'_l(t)| + |\phi''_k(t) - \phi''_l(t)| &\leq |\phi'_k(t) - \xi| + |\xi - \phi'_l(t)| + |\phi''_k(t) - \lambda| + |\lambda - \phi''_l(t)| \\ &< d + d = 2d, \end{aligned}$$

which contradicts the separation condition of $\mathcal{A}_{\epsilon, \Delta}$. \square

Lemma 4. If $(t, \xi, \lambda) \notin Z_k$, then

$$\left| T_{f_k}^{(x^n g)}(t, \xi, \lambda) \right| \leq \epsilon E_{k,n}(t),$$

where $E_{k,n}(t) := \|\phi'_k\|_{L^\infty} I_{n+1} + (D_n + \frac{\pi}{3} \|\phi'_k\|_{L^\infty} I_{n+3}) A_k(t)$. Consequently, for any $(t, \xi, \lambda) \in Z_k$, we have

$$\left| T_f^{(x^n g)}(t, \xi, \lambda) - T_{f_k}^{(x^n g)}(t, \xi, \lambda) \right| \leq \epsilon \sum_{l \neq k} E_{l,n}(t).$$

Proof. Using second order Taylor expansion of ϕ_k , we can write

$$\begin{aligned} f_k(x) &= A_k(x) e^{2\pi i \phi_k(x)} \\ &= (A_k(x) - A_k(t)) e^{2\pi i \phi_k(x)} + A_k(t) e^{2\pi i [\phi_k(t) + \phi'_k(t)(x-t) + \frac{1}{2} \phi''_k(t)(x-t)^2]} \\ &\quad + A_k(t) (e^{2\pi i \phi_k(x)} - e^{2\pi i [\phi_k(t) + \phi'_k(t)(x-t) + \frac{1}{2} \phi''_k(t)(x-t)^2]}). \end{aligned}$$

Denote these three terms in the sum by $f_{k,1}, f_{k,2}, f_{k,3}$ respectively. Then we have

$$\begin{aligned} \left| T_{f_{k,1}}^{(x^n g)}(t, \xi, \lambda) \right| &\leq \int |A_k(x) - A_k(t)| |x-t|^n |g(x-t)| dx \\ &\leq \epsilon \|\phi'_k\|_{L^\infty} \int |x-t|^{n+1} |g(x-t)| dx \\ &\leq \epsilon \|\phi'_k\|_{L^\infty} I_{n+1}, \end{aligned}$$

and if $(t, \xi, \lambda) \notin Z_k$, then

$$\begin{aligned} \left| T_{f_{k,2}}^{(x^n g)}(t, \xi, \lambda) \right| &= A_k(t) \left| (x^n g)(\xi - \phi'_k(t), \lambda - \phi''_k(t)) \right| \\ &\leq A_k(t) D_n \epsilon. \end{aligned}$$

For $f_{k,3}$, we have

$$\begin{aligned} \left| T_{f_{k,3}}^{(x^n g)}(t, \xi, \lambda) \right| &\leq A_k(t) \int \frac{\pi}{3} \|\phi_k'''\|_{L^\infty} |x-t|^{n+3} |g(x-t)| dx \\ &\leq \epsilon \frac{\pi}{3} A_k(t) \|\phi'_k\|_{L^\infty} I_{n+3}. \end{aligned}$$

Therefore, for $(t, \xi, \lambda) \notin Z_k$,

$$\left| T_{f_k}^{(x^n g)}(t, \xi, \lambda) \right| \leq \epsilon \left[\|\phi'_k\|_{L^\infty} I_{n+1} + (D_n + \frac{\pi}{3} \|\phi'_k\|_{L^\infty} I_{n+3}) A_k(t) \right].$$

Consequently,

$$\left| T_f^{(x^n g)}(t, \xi, \lambda) - T_{f_k}^{(x^n g)}(t, \xi, \lambda) \right| \leq \sum_{l \neq k} E_{l,n}(t).$$

□

Since for each k , $E_{k,0}(t)$ is uniformly bounded from above and from below for all $(t, \xi, \lambda) \notin Z_k$, it follows that if ϵ is sufficiently small, such that for all $(t, \xi, \lambda) \notin \bigcup_{k=1}^K Z_k$,

$$\epsilon \leq \left(\sum_{k=1}^K E_{k,0}(t) \right)^{-\frac{6}{5}},$$

then for any $(t, \xi, \lambda) \notin \bigcup_{k=1}^K Z_k$, $\left| T_f^{(g)}(t, \xi, \lambda) \right| \leq \tilde{\epsilon}$.

To simplify the notation, we omit (t, ξ, λ) in $T_f^{(g)}(t, \xi, \lambda)$ in following lemmas and proofs.

Lemma 5. If $(t, \xi, \lambda) \in Z_k$ for some k , $1 \leq k \leq K$, then

$$(10) \quad \left| \partial_t T_f^{(g)} - 2\pi i (\phi'_k(t) T_f^{(g)} + \phi''_k(t) T_f^{(xg)}) \right| \leq \epsilon B_{k,1}(t),$$

where

$$\begin{aligned} B_{k,1}(t) &:= \sum_{k=1}^K \left\| \phi'_k \right\|_{L^\infty} (I_0 + \pi \|A_k\|_{L^\infty} I_2) + 2\pi \sum_{l \neq k} (\phi'_l(t) E_{l,0}(t) + |\phi''_l(t)| E_{l,1}(t)) \\ &\quad + 2\pi (\phi'_k(t) \sum_{l \neq k} E_{l,0}(t) + |\phi''_k(t)| \sum_{l \neq k} E_{l,1}(t)). \end{aligned}$$

Proof. If $(t, \xi, \lambda) \notin Z_k$, then

$$\begin{aligned} \partial_t T_f^{(g)} &= \partial_t \left(\sum_{k=1}^K \int A_k(x) e^{2\pi i \phi_k(x)} g(x-t) e^{-2\pi i \xi(x-t) - \pi i \lambda(x-t)^2} dx \right) \\ &= \sum_{k=1}^K \left[\int A'_k(x) e^{2\pi i \phi_k(x)} g(x-t) e^{-2\pi i \xi(x-t) - \pi i \lambda(x-t)^2} dx \right. \\ &\quad \left. + \int A_k(x) 2\pi i \phi'_k(x) e^{2\pi i \phi_k(x)} g(x-t) e^{-2\pi i \xi(x-t) - \pi i \lambda(x-t)^2} dx \right] \\ &= \sum_{k=1}^K \left[\int A'_k(x) e^{2\pi i \phi_k(x)} g(x-t) e^{-2\pi i \xi(x-t) - \pi i \lambda(x-t)^2} dx \right. \\ &\quad \left. + \int A_k(x) 2\pi i \left[\phi'_k(t) + \phi''_k(t)(x-t) + \int_0^{x-t} (\phi''_k(t+u) - \phi''_k(t)) du \right] \right. \\ &\quad \left. \times e^{2\pi i \phi_k(x)} g(x-t) e^{-2\pi i \xi(x-t) - \pi i \lambda(x-t)^2} dx \right]. \end{aligned}$$

It follows that

$$\begin{aligned}
& \left| \partial_t T_f^{(g)} - 2\pi i \sum_{k=1}^K (\phi'_k(t) T_{f_k}^{(g)} + \phi''_k(t) T_{f_k}^{(xg)}) \right| \\
& \leq \sum_{k=1}^K \left[\int |A'_k(x)| |g(x-t)| dx + 2\pi \int A_k(x) \left| \int_0^{x-t} [\phi''_k(t+u) - \phi''_k(t)] du \right| |g(x-t)| dx \right] \\
& \leq \sum_{k=1}^K (\epsilon \|\phi'_k\|_{L^\infty} I_0 + \pi \|\phi''_k\|_{L^\infty} \|A_k\|_{L^\infty} I_2) \\
& \leq \epsilon \sum_{k=1}^K \|\phi'_k\|_{L^\infty} (I_0 + \pi \|A_k\|_{L^\infty} I_2).
\end{aligned}$$

By Lemma 4, when $(t, \xi, \lambda) \in Z_k$, we have

$$\begin{aligned}
& \left| \partial_t T_f^{(g)} - 2\pi i (\phi'_k(t) T_{f_k}^{(g)} + \phi''_k(t) T_{f_k}^{(xg)}) \right| \\
& \leq \epsilon \left(\sum_{k=1}^K \|\phi'_k\|_{L^\infty} (I_0 + \pi \|A_k\|_{L^\infty} I_2) + 2\pi \sum_{l \neq k} (\phi'_l(t) E_{l,0}(t) + |\phi''_l(t)| E_{l,1}(t)) \right),
\end{aligned}$$

so finally we have

$$\begin{aligned}
& \left| \partial_t T_f^{(g)} - 2\pi i (\phi'_k(t) T_f^{(g)} + \phi''_k(t) T_f^{(xg)}) \right| \\
& \leq \epsilon \left(\sum_{k=1}^K \|\phi'_k\|_{L^\infty} (I_0 + \pi \|A_k\|_{L^\infty} I_2) + 2\pi \sum_{l \neq k} (\phi'_l(t) E_{l,0}(t) + |\phi''_l(t)| E_{l,1}(t)) \right) \\
& \quad + 2\pi (\phi'_k(t) \sum_{l \neq k} E_{l,0}(t) + |\phi''_k(t)| \sum_{l \neq k} E_{l,1}(t)).
\end{aligned}$$

□

Lemma 6. If $(t, \xi, \lambda) \in Z_k$, then

$$\left| \partial_{tt}^2 T_f^{(g)} - 2\pi i (\phi''_k(t) T_f^{(g)} + \phi'_k(t) \partial_t T_f^{(g)} + \phi''_k(t) \partial_t T_f^{(xg)}) \right| \leq \epsilon B_{k,2}(t),$$

where

$$\begin{aligned}
B_{k,2}(t) & := \Omega_2 + 2\pi \sum_{l \neq k} (|\phi''_l(t)| E_{l,0}(t) + \phi'_l(t) F_{l,0}(t) + \phi''_l(t) F_{l,1}(t)) \\
& \quad + 2\pi (|\phi''_k(t)| \sum_{l \neq k} E_{l,0}(t) + \phi'_k(t) \sum_{l \neq k} F_{l,0}(t) + \phi''_k(t) \sum_{l \neq k} F_{l,1}(t)),
\end{aligned}$$

with

$$\Omega_2 := \sum_{k=1}^K \left[\|\phi'_k\|_{L^\infty} I_0 + 2\pi \|A_k\|_{L^\infty} \|\phi'_k\|_{L^\infty} I_1 + 2\pi \|\phi'_k\|_{L^\infty}^2 I_0 + \pi (\|A'_k\|_{L^\infty} + 2\pi \|\phi'_k\|_{L^\infty} \|A_k\|_{L^\infty}) I_2 \right],$$

and

$$F_{l,n}(t) := \|\phi'_l\|_{L^\infty} (I_n + \pi \|A_l\|_{L^\infty} I_{n+2}) + 2\pi (\phi'_l(t) E_{l,n}(t) + |\phi''_l(t)| E_{l,n+1}(t)).$$

Proof.

$$\begin{aligned}
\partial_{tt}^2 T_f^{(g)} &= \sum_{k=1}^K \int (A_k''(x) + 4\pi i \phi_k'(x) A_k'(x) + 2\pi i \phi_k''(x) A_k(x) - 4\pi^2 \phi_k'(x)^2 A_k(x)) \\
&\quad e^{2\pi i \phi_k(x)} g(x-t) e^{-2\pi i \xi(x-t) - \pi i \lambda(x-t)^2} dx \\
&= \sum_{k=1}^K \left(\int A_k''(x) e^{2\pi i \phi_k(x)} g(x-t) e^{-2\pi i \xi(x-t) - \pi i \lambda(x-t)^2} dx \right. \\
&\quad + 2\pi i \int \phi_k''(x) A_k(x) e^{2\pi i \phi_k(x)} g(x-t) e^{-2\pi i \xi(x-t) - \pi i \lambda(x-t)^2} dx \\
&\quad + 2\pi i \int \phi_k'(x) A_k'(x) e^{2\pi i \phi_k(x)} g(x-t) e^{-2\pi i \xi(x-t) - \pi i \lambda(x-t)^2} dx \\
&\quad \left. + 2\pi i \int \phi_k'(x) f_k'(x) e^{2\pi i \phi_k(x)} g(x-t) e^{-2\pi i \xi(x-t) - \pi i \lambda(x-t)^2} dx \right).
\end{aligned}$$

The first term gives

$$\left| \sum_{k=1}^K \int A_k''(x) e^{2\pi i \phi_k(x)} g(x-t) e^{-2\pi i \xi(x-t) - \pi i \lambda(x-t)^2} dx \right| \leq \epsilon \sum_{k=1}^K \|\phi_k'\|_{L^\infty} I_0;$$

and the second term gives

$$\begin{aligned}
&\left| 2\pi i \sum_{k=1}^K \int \phi_k''(x) A_k(x) e^{2\pi i \phi_k(x)} g(x-t) e^{-2\pi i \xi(x-t) - \pi i \lambda(x-t)^2} dx - 2\pi i \sum_{k=1}^K \phi_k''(t) V_{f_k}^{(g)} \right| \\
&\leq 2\pi \sum_{k=1}^K \int \epsilon \|\phi_k'\|_{L^\infty} |x-t| |A_k(x)| |g(x-t)| dx \\
&\leq 2\pi \epsilon I_1 \sum_{k=1}^K \|A_k\|_{L^\infty} \|\phi_k'\|_{L^\infty};
\end{aligned}$$

and the third term gives

$$\left| 2\pi i \sum_{k=1}^K \int \phi_k'(x) A_k'(x) e^{2\pi i \phi_k(x)} g(x-t) e^{-2\pi i \xi(x-t) - \pi i \lambda(x-t)^2} dx \right| \leq 2\pi \epsilon \sum_{k=1}^K \|\phi_k'\|_{L^\infty}^2 I_0;$$

and for the last term, note that $\partial_t V_{f_k}^{(g)} = V_{f_k}^{(g)}$ and $\partial_t V_{f_k}^{(xg)} = V_{f_k}^{(xg)}$, by the second order Taylor expansion of $\phi_k'(x)$, we have

$$\begin{aligned}
&\left| 2\pi i \sum_{k=1}^K \int \phi_k'(x) f_k'(x) e^{2\pi i \phi_k(x)} g(x-t) e^{-2\pi i \xi(x-t) - \pi i \lambda(x-t)^2} dx - 2\pi i \sum_{k=1}^K (\phi_k'(t) \partial_t V_{f_k}^{(g)} + \phi_k''(t) \partial_t V_{f_k}^{(xg)}) \right| \\
&\leq 2\pi \left| \sum_{k=1}^K \int \frac{1}{2} \|\phi_k'''\|_{L^\infty} (x-t)^2 (A_k'(x) + 2\pi i \phi_k'(x) A_k(x)) e^{2\pi i \phi_k(x)} g(x-t) e^{-2\pi i \xi(x-t) - \pi i \lambda(x-t)^2} dx \right| \\
&\leq \pi \epsilon \sum_{k=1}^K (\|A_k'\|_{L^\infty} + 2\pi \|\phi_k'\|_{L^\infty} \|A_k\|_{L^\infty}) I_2.
\end{aligned}$$

Combine those estimates above, and we have

$$\left| \partial_{tt}^2 T_f^{(g)} - 2\pi i \sum_{k=1}^K (\phi_k''(t) V_{f_k}^{(g)} + \phi_k'(t) \partial_t V_{f_k}^{(g)} + \phi_k''(t) \partial_t V_{f_k}^{(xg)}) \right| \leq \epsilon \Omega_2,$$

From the proof of Lemma 5, we know that

$$\left| \partial_t T_{f_i}^{(g)} - 2\pi i (\phi_i'(t) T_{f_i}^{(g)} + \phi_i''(t) T_{f_i}^{(xg)}) \right| \leq \epsilon \|\phi_i'\|_{L^\infty} (I_0 + \pi \|A_l\|_{L^\infty} I_2),$$

$$\left| \partial_t T_{f_i}^{(xg)} - 2\pi i (\phi_i'(t) T_{f_i}^{(xg)} + \phi_i''(t) T_{f_i}^{(x^2g)}) \right| \leq \epsilon \|\phi_i'\|_{L^\infty} (I_1 + \pi \|A_l\|_{L^\infty} I_3).$$

So using Lemma 4, if $(t, \xi, \lambda) \in Z_k$, for $l \neq k$, we have

$$\begin{aligned} \left| \partial_t T_{f_l}^{(g)} \right| &\leq \epsilon \left[\|\phi_l'\|_{L^\infty} (I_0 + \pi \|A_l\|_{L^\infty} I_2) + 2\pi (\phi_l'(t) E_{l,0}(t) + |\phi_l''(t)| E_{l,1}(t)) \right] \\ &= \epsilon F_{l,0}(t), \end{aligned}$$

and

$$\begin{aligned} \left| \partial_t T_{f_l}^{(xg)} \right| &\leq \epsilon \left[\|\phi_l'\|_{L^\infty} (I_1 + \pi \|A_l\|_{L^\infty} I_3) + 2\pi (\phi_l'(t) E_{l,1}(t) + |\phi_l''(t)| E_{l,2}(t)) \right] \\ &= \epsilon F_{l,1}(t). \end{aligned}$$

Therefore, for $(t, \xi, \lambda) \in Z_k$, we have

$$\left| \partial_t T_f^{(g)} - \partial_t T_{f_k}^{(g)} \right| \leq \epsilon \sum_{l \neq k} F_{l,0}(t),$$

and

$$\left| \partial_t T_f^{(xg)} - \partial_t T_{f_k}^{(xg)} \right| \leq \epsilon \sum_{l \neq k} F_{l,1}(t).$$

We then get, for $(t, \xi, \lambda) \in Z_k$

$$\begin{aligned} &\left| \partial_{tt}^2 T_f^{(g)} - 2\pi i (\phi_k''(t) V_f^{(g)} + \phi_k'(t) \partial_t V_f^{(g)} + \phi_k''(t) \partial_t V_f^{(xg)}) \right| \\ &\leq \left| \partial_{tt}^2 T_f^{(g)} - 2\pi i \sum_{k=1}^K (\phi_k''(t) V_{f_k}^{(g)} + \phi_k'(t) \partial_t V_{f_k}^{(g)} + \phi_k''(t) \partial_t V_{f_k}^{(xg)}) \right| \\ &\quad + \left| 2\pi i \sum_{l \neq k} (\phi_l''(t) V_{f_l}^{(g)} + \phi_l'(t) \partial_t V_{f_l}^{(g)} + \phi_l''(t) \partial_t V_{f_l}^{(xg)}) \right| \\ &\quad + \left| 2\pi i \left[\phi_k''(t) (V_f^{(g)} - V_{f_k}^{(g)}) + \phi_k'(t) (\partial_t T_f^{(g)} - \partial_t T_{f_k}^{(g)}) + \phi_k''(t) (\partial_t T_f^{(xg)} - \partial_t T_{f_k}^{(xg)}) \right] \right| \\ &\leq \epsilon \left(\Omega_2 + 2\pi \sum_{l \neq k} (|\phi_l''(t)| E_{l,0}(t) + \phi_l'(t) F_{l,0}(t) + \phi_l''(t) F_{l,1}(t)) \right. \\ &\quad \left. + 2\pi (|\phi_k''(t)| \sum_{l \neq k} E_{l,0}(t) + \phi_k'(t) \sum_{l \neq k} F_{l,0}(t) + \phi_k''(t) \sum_{l \neq k} F_{l,1}(t)) \right). \end{aligned}$$

□

Lemma 7. For any $(t, \xi, \lambda) \in Z_k$, such that $\left|T_f^{(g)}(t, \xi, \lambda)\right| > \tilde{\epsilon}$ and $2\pi \left|1 + \partial_t \left(\frac{T_f^{(xg)}(t, \xi, \lambda)}{T_f^{(g)}(t, \xi, \lambda)}\right)\right| > \tilde{\epsilon}$, we have

$$\left|\mu_f^{(g)}(t, \xi, \lambda) - \phi_k''(t)\right| \leq \tilde{\epsilon},$$

provided ϵ is sufficiently small.

Proof. First, for any (t, ξ, λ) satisfies the conditions of the lemma, we have

$$\left|2\pi i(T_f^{(g)})^2 + 2\pi i(T_f^{(g)} \partial_t T_f^{(xg)} - T_f^{(xg)} \partial_t T_f^{(g)})\right| = 2\pi \left|1 + \partial_t \left(\frac{T_f^{(xg)}}{T_f^{(g)}}\right)\right| \left|T_f^{(g)}\right|^2 > \tilde{\epsilon}^3.$$

By Lemma 5 and 6, for $(t, \xi, \lambda) \in Z_k$, we have

$$\begin{aligned} & \left|\mu_f^{(g)}(t, \xi, \lambda) - \phi_k''(t)\right| \\ &= \left|\phi_k''(t) - \frac{T_f^{(g)} \partial_{tt}^2 T_f^{(g)} - (\partial_t T_f^{(g)})^2}{2\pi i(T_f^{(g)})^2 + 2\pi i(T_f^{(g)} \partial_t T_f^{(xg)} - T_f^{(xg)} \partial_t T_f^{(g)})}\right| \\ &= \left|\frac{\partial_t T_f^{(g)} \left[\partial_t T_f^{(g)} - 2\pi i \phi_k''(t) T_f^{(xg)} - 2\pi i \phi_k'(t) T_f^{(g)}\right]}{2\pi i(T_f^{(g)})^2 + 2\pi i(T_f^{(g)} \partial_t T_f^{(xg)} - T_f^{(xg)} \partial_t T_f^{(g)})}\right. \\ & \quad \left. - \frac{T_f^{(g)} \left[\partial_{tt}^2 T_f^{(g)} - 2\pi i \phi_k''(t) T_f^{(g)} - 2\pi i \phi_k'(t) \partial_t T_f^{(g)} - 2\pi i \phi_k''(t) \partial_t T_f^{(xg)}\right]}{2\pi i(T_f^{(g)})^2 + 2\pi i(T_f^{(g)} \partial_t T_f^{(xg)} - T_f^{(xg)} \partial_t T_f^{(g)})}\right| \\ &\leq \epsilon B_{k,1}(t) \left|\frac{\partial_t T_f^{(g)}}{2\pi i(T_f^{(g)})^2 + 2\pi i(T_f^{(g)} \partial_t T_f^{(xg)} - T_f^{(xg)} \partial_t T_f^{(g)})}\right| \\ &\quad + \epsilon B_{k,2}(t) \left|\frac{T_f^{(g)}}{2\pi i(T_f^{(g)})^2 + 2\pi i(T_f^{(g)} \partial_t T_f^{(xg)} - T_f^{(xg)} \partial_t T_f^{(g)})}\right| \\ &\leq \tilde{\epsilon}^3 (B_{k,1}(t) \left|\partial_t T_f^{(g)}\right| + B_{k,2}(t) \left|T_f^{(g)}\right|). \end{aligned}$$

By the uniform boundedness of $B_{k,n}(t)$, $\left|\partial_t T_f^{(g)}\right|$ and $\left|T_f^{(g)}\right|$, if we impose an extra restriction on ϵ , namely that, for all $k \in \{1, \dots, K\}$ and all $(t, \xi, \lambda) \in Z_k$,

$$\epsilon \leq (B_{k,1}(t) \left|\partial_t T_f^{(g)}\right| + B_{k,2}(t) \left|T_f^{(g)}\right|)^{-3},$$

then $\left|\mu_f^{(g)}(t, \xi, \lambda) - \phi_k''(t)\right| \leq \tilde{\epsilon}$. □

Lemma 8. For any $(t, \xi, \lambda) \in Z_k$, such that $\left|T_f^{(g)}(t, \xi, \lambda)\right| > \tilde{\epsilon}$ and $2\pi \left|1 + \partial_t \left(\frac{T_f^{(xg)}(t, \xi, \lambda)}{T_f^{(g)}(t, \xi, \lambda)}\right)\right| > \tilde{\epsilon}$, we have

$$\left|\omega_f^{(g)}(t, \xi, \lambda) - \phi_k'(t)\right| \leq \tilde{\epsilon},$$

provided ϵ is sufficiently small.

Proof. By Lemma 5 and 7, for $(t, \xi, \lambda) \in Z_k$, we have

$$\begin{aligned}
\left| \omega_f^{(g)}(t, \xi, \lambda) - \phi_k'(t) \right| &= \left| \frac{\partial_t T_f^{(g)} - 2\pi i \mu_f^{(g)} T_f^{(xg)}}{2\pi i T_f^{(g)}} - \phi_k'(t) \right| \\
&= \left| \frac{\partial_t T_f^{(g)} - 2\pi i \phi_k'(t) T_f^{(g)} - 2\pi i \phi_k''(t) V_f^{(xg)}}{2\pi i T_f^{(g)}} + \frac{(\phi_k''(t) - \mu_f^{(g)}) T_f^{(xg)}}{T_f^{(g)}} \right| \\
&\leq \left| \frac{\partial_t T_f^{(g)} - 2\pi i \phi_k'(t) T_f^{(g)} - 2\pi i \phi_k''(t) V_f^{(xg)}}{2\pi i T_f^{(g)}} \right| + \left| \frac{(\phi_k''(t) - \mu_f^{(g)}) T_f^{(xg)}}{T_f^{(g)}} \right| \\
&\leq \frac{\tilde{\epsilon}^5 B_{k,1}(t)}{2\pi} + \tilde{\epsilon}^2 (B_{k,1}(t) \left| \partial_t T_f^{(g)} \right| + B_{k,2}(t) \left| T_f^{(g)} \right|) \left| T_f^{(xg)} \right|.
\end{aligned}$$

By a similar argument as in the proof of Lemma 7, $\left| \omega_f^{(g)}(t, \xi, \lambda) - \phi_k'(t) \right| \leq \tilde{\epsilon}$, if ϵ is sufficiently small. \square

DEPARTMENT OF MATHEMATICS, DUKE UNIVERSITY, DURHAM, NC, USA
Email address: ziyu@math.duke.edu

DEPARTMENT OF MATHEMATICS AND DEPARTMENT OF STATISTICAL SCIENCE, DUKE UNIVERSITY, DURHAM, NC, USA. MATHEMATICS DIVISION, NATIONAL CENTER FOR THEORETICAL SCIENCES, TAIPEI, TAIWAN
Email address: hauwu@math.duke.edu